nature communications

Article

https://doi.org/10.1038/s41467-026-73579-y

Single-atom substitution redirects KatG reactivity from cofactor biogenesis to stereoselective sulfoxidation

Received: 23 February 2026

Accepted: 14 May 2026

Published online: xx xx 2026

Check for updates

Ran Duan[1], Jiasong Li[1,4], Wendell P. Griffith[1], Yang Xu[2], Nathan D. Burrows[2], Anthony P. Green[3] & Aimin Liu[1,5]

Protein-derived cofactors rely on precisely positioned heteroatoms to direct redox chemistry, yet isolating their individual contributions remains challenging. The indole N–H of tryptophan plays a central yet elusive role in biogenesis and function of the Met–Tyr–Trp (MYW) cofactor in catalase-peroxidase (KatG). Here, we use genetic code expansion to replace cofactor-forming Trp105 with thiotryptophan (S-Trp), enabling a single-heteroatom (N → S) substitution. Instead of forming the MYW crosslink, KatG bearing S-Trp105 undergoes site-specific monooxygenation to yield a chiral sulfoxide. HPLC-MS, circular dichroism, and FT-IR spectroscopy identify selective oxygen insertion at the sulfur, establishing enantioselective formation of an (*S*)-configured sulfoxide. A 2.22 Å cryo-EM structure visualizes the oxidized S-Trp105, revealing the S = O moiety orienting toward the iron and confirming the absence of crosslinking. The S-atom oxygenation is heme-dependent and proceeds via a two-electron oxygen-atom transfer, contrasting with the radical-mediated one-electron chemistry of native tryptophan. This redirection suppresses catalase activity by perturbing cofactor formation. These results show that a single-atom substitution reroutes the distal heme site from radical crosslinking to stereoselective sulfoxidation, uncovering a monooxygenase-like capability within KatG. This work highlights using non-canonical amino acids to achieve atomic-level control over reaction pathways and to interrogate cofactor biogenesis with unprecedented precision.

Catalase-peroxidase (KatG) is a bifunctional enzyme broadly distributed across archaea, bacteria, and lower eukaryotes[1]. KatG combines a high-turnover catalase activity, catalyzing the disproportionation of hydrogen peroxide (H_2O_2) at rates of several thousand turnovers per second, with a slower peroxidase activity that oxidizes diverse substrates using H_2O_2 as the oxidant[2,3]. The catalase function critically depends on a protein-derived cofactor formed by a covalently crosslinked triad of methionine, tyrosine, and tryptophan side chains (MYW), whereas the peroxidase activity relies solely on the heme center[4]. In pathogenic organisms, the catalase activity of KatG is essential for survival within the host, where detoxification of H_2O_2 produced by the immune response is required for persistence and virulence[5,6].

Q1 – Q5

[1]Department of Chemistry, The University of Texas at San Antonio, San Antonio, TX 78249, USA. [2]Division of CryoEM and Bioimaging, Stanford Synchrotron Radiation Lightsource, SLAC National Accelerator Laboratory, Stanford University, Menlo Park, CA 94025, USA. [3]Manchester Institute of Biotechnology and Department of Chemistry, The University of Manchester, Manchester M1 7DN, UK. [4]Present address: Key Laboratory of Agricultural Environmental Microbiology, Ministry of Agriculture, College of Life Sciences, Nanjing Agricultural University, Nanjing 210095, P. R. China. [5]Present address: Department of Biochemistry and Biophysics, and Department of Chemistry, University of Pennsylvania, Philadelphia, PA 19104, USA. e-mail: Feradical@utsa.edu

In contrast to monofunctional heme catalases, KatG employs the MYW cofactor to enable catalase activity through a protein-based radical mechanism (Fig. 1A). The MYW triad represents one of the most structurally and mechanistically intricate protein-derived cofactors known thus far, as its formation requires autocatalytic crosslinking of residues drawn from three distant regions of the polypeptide chain[7]. Elucidating the biosynthesis and function of MYW has proven challenging: cofactor formation occurs only once per polypeptide, generates weak and spectrally congested optical signatures, and is difficult to observe directly in intact protein[8]. Previous studies using heme-free KatG demonstrated that MYW formation can be initiated upon heme reconstitution followed by peroxide treatment, establishing that cofactor biogenesis is tightly coupled to heme-dependent oxidative chemistry[8,9].

Structural and spectroscopic studies have revealed an alternative natural form of the triad, MYW–OOH, in which the indole nitrogen of tryptophan is peroxygenated (Fig. 1B). This species has been observed crystallographically in as-isolated KatGs from multiple organisms[6,10,11] and, more recently, detected in solution as the predominant form of *Mycobacterium tuberculosis* (Mtb) KatG cultured under ambient conditions[11]. These observations highlight the functional importance of the indole N–H of tryptophan. Although the indole nitrogen is the closest heavy atom of the MYW cofactor to the heme iron, it is still more than 4 Å away. Its position and chemical properties therefore support a role in hydrogen atom transfer (HAT) steps[1,11–15], which initiate the radical-mediated crosslink formation during MYW biogenesis (Supplementary Fig. 1)[8,9,16,17].

During catalytic turnover promoted by KatG, the MYW catalytic triad is oxidized to the MYW$^{\bullet}$, via the indole nitrogen[5,6], which is believed to be essential for catalase function, as it retains the oxidizing equivalent in the distal heme pocket, allowing it to oxidize the next H_2O_2 rather than oxidizing a peroxidatic donor via the radical propagation pathway[16]. Despite its centrality, direct experimental interrogation of the indole N–H group in these processes has remained elusive.

Traditional site-directed mutagenesis has been the primary strategy for studying protein-derived cofactors. However, this approach is intrinsically limited for autocatalytically formed crosslinks such as MYW. Substitution of any cofactor-forming residue typically abolishes cofactor formation entirely, yielding variants that report only on loss of function rather than on mechanistic detail[7]. As a result, protein-derived radical cofactors have been largely inaccessible to systematic structure-function interrogation at the atomic level. To overcome these limitations, genetic code expansion has emerged as a powerful strategy to introduce noncanonical amino acids (ncAAs) site-specifically into proteins[18]. We and others have shown that this approach enables controlled perturbation of autocatalytically formed cofactors, including Cys–Tyr dyads in iron- and copper-containing enzymes, providing mechanistic insights unattainable by canonical mutagenesis[19–22].

Here, we apply genetic code expansion to KatG by replacing the MYW-forming tryptophan with the sulfur-containing analog thiotryptophan (3-benzothienyl-L-alanine, S-Trp)[23,24]. This single-atom NH → S substitution preserves aromaticity while altering hydrogen-bonding capacity and redox chemistry, offering a precise means to redirect oxidative reactivity at a critical catalytic position. Rather than yielding a simple loss-of-function variant, S-Trp substitution reveals an unexpected alternative reaction pathway that illuminates how KatG controls radical versus two-electron oxidation chemistry at the protein–heme interface.

Results

Single-atom substitution at Trp105 redirects KatG catalytic function

To interrogate how the cofactor-forming tryptophan contributes to KatG reactivity, we replaced Trp105 in *Escherichia coli* KatG (EcKatG) with thiotryptophan (β-[3-benzo(b)thienyl]-L-alanine, S-Trp) using genetic code expansion. EcKatG was selected for its robust heterologous expression and well-characterized catalytic properties[25]. S-Trp closely mimics the steric and aromatic features of tryptophan, with a benzothiophene ring system in which sulfur replaces the indole nitrogen. Critically, this NH → S substitution preserves aromaticity while eliminating the indole N–H proton, thereby precluding hydrogen atom transfer from this position. This single-atom modification provides a precise means to redirect redox chemistry at Trp105 without grossly perturbing protein structure. Using a high-fidelity engineered pyrrolysyl-tRNA synthetase (PylRS)/tRNA pair specific for S-Trp[24], we achieved efficient and site-specific incorporation of S-Trp at position 105 (Supplementary Fig. 2).

Although Trp105 is located several angstroms from the heme iron, substitution with S-Trp produces measurable changes in the optical properties of KatG. The S-Trp105 variant exhibits a red-shifted Soret

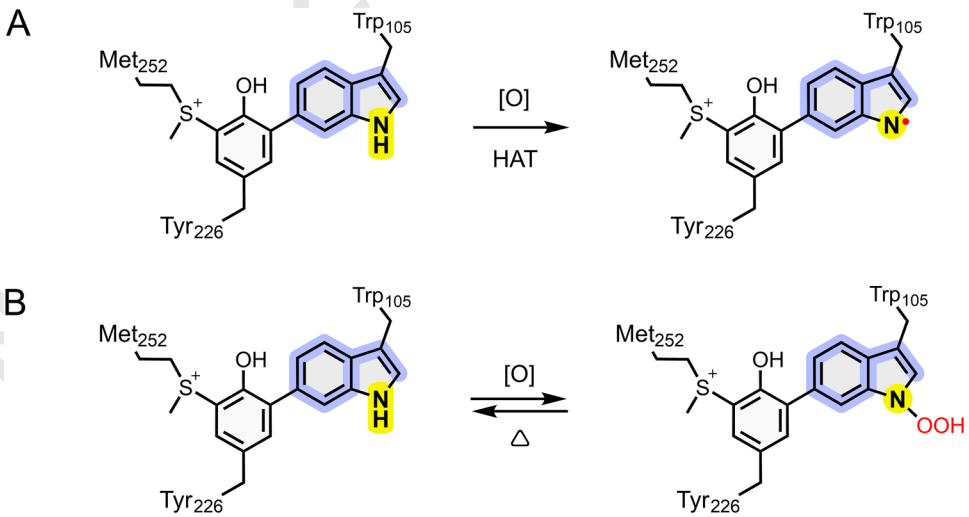

Fig. 1 | The indole N–H moiety of the protein-derived MYW cofactor in KatG is the critical oxidation hub for KatG reactivity. A The indole N-H moiety is proposed to be essential for hydrogen atom transfer (HAT) that elevates the MYW oxidation state and drives the catalase cycle. **B** The protein-derived cofactor in KatG is also naturally present in an oxygenated form with oxygen inserted into the indole N–H moiety, MYW-OOH, allowing the cofactor to enter a reversible, catalase-dormant yet primed state.

https://doi.org/10.1038/s41467-026-73579-y

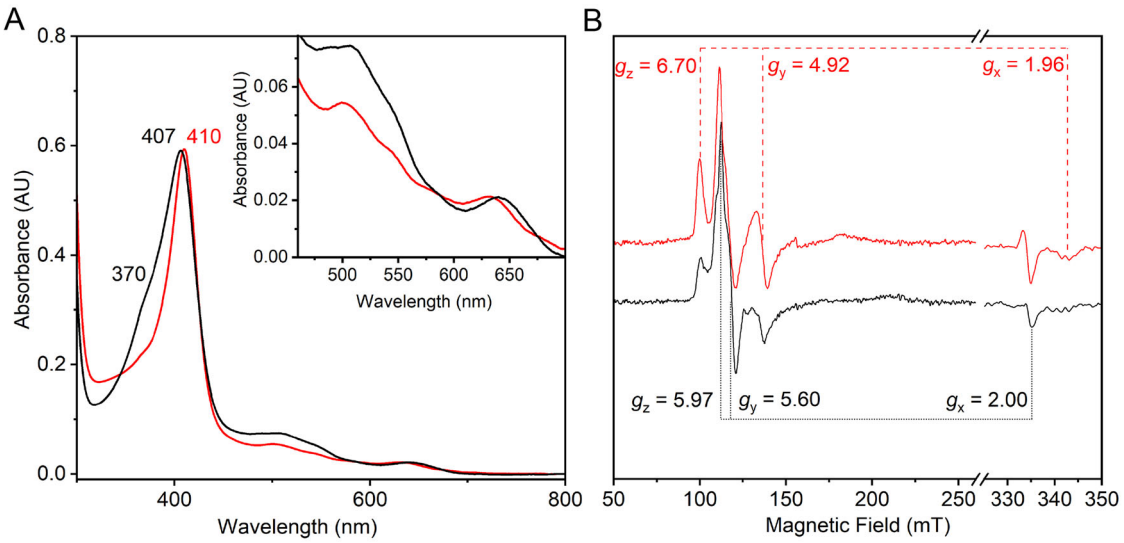

Fig. 2 | Substitution of the indole nitrogen with sulfur results in changes to the heme electronic environment. A UV-vis spectra of WT KatG (black) and KatG S-Trp105 (red) showing a red shift of the Soret band from 407 to 410 nm and attenuation of the visible-region absorbance feature. The insignificant differences of the α/β (Q-) bands are shown in an inset. **B** Comparison of the 10 K EPR spectra of WT KatG (black) and KatG S-Trp105 (red). Both spectra show a mixture of two high-spin ferric heme signals.

maximum, 410 versus 407 nm in wild-type (WT) (Fig. 2A), and lacks the ~370 nm shoulder observed in some KatGs and associated with cofactor-related electronic transitions[11]. In contrast, continuous-wave X-band EPR spectra of the S-Trp105 variant are essentially indistinguishable from those of the WT enzyme (Fig. 2B), indicating that the heme iron spin state and ligand field symmetry remain intact. Together, these data indicate that the NH → S substitution at Trp105 induces subtle but detectable perturbations of the heme electronic environment, detectable by UV-vis spectroscopy yet insufficient to alter the paramagnetic properties probed by EPR spectroscopy.

Functional assays reveal that site-specific substitution of Trp with S-Trp profoundly alters KatG catalytic behavior

The S-Trp105 variant displays an approximately 10^3-fold decrease in catalase activity relative to WT KatG (Table 1). It also exhibits lower activity than the Y226F variant, which is incapable of forming the MYW cofactor (Supplementary Fig. 3). Together, these observations indicate effective suppression of MYW-dependent catalysis. Peroxidase activity is also reduced, with the S-Trp105 variant retaining approximately 6.3% of WT activity (Table 1). The magnitude and pattern of these changes are consistent with the effective suppression of MYW-dependent catalysis, while the specific retention of residual peroxidase activity prompted our investigation into the alternative reaction pathway characterized in the following section.

Spectroscopic and mass spectrometric evidence for site-specific sulfur oxygenation

Tryptic digests of S-Trp–incorporated KatG and the WT enzyme were analyzed by HPLC coupled with optical detection. As expected, WT KatG produced the characteristic Met–Tyr–Trp (MYW) crosslinked peptide fragment (CLPF), which exhibits a diagnostic absorption maximum at 330 nm and the predicted *m/z* value, eluting at a retention time consistent with previous reports for KatG cofactors (Supplementary Fig. 4)[9]. In contrast, no peptide corresponding to the MYW-containing CLPF was detected at this retention time in the S-Trp105 KatG digest (Supplementary Fig. 5). Instead, a distinct peptide eluted at 40.77 min and displayed absorption maxima at 277 and 318 nm (Fig. 3A), indicative of a chemically modified aromatic residue within the same sequence context.

Table 1 | Catalase and peroxidase kinetic parameters

Catalase activity	**k_{cat} (s^{-1})**	**K_M (mM)**	**k_{cat}/K_M ($s^{-1}M^{-1}$)**
WT KatG	3900 ± 10	2.1 ± 0.2	(19 ± 2) x 10^5
KatG S-Trp105	7.3 ± 0.2	8.3 ± 0.4	900 ± 50
KatG Y226F	13 ± 0.2	3.5 ± 0.2	3700 ± 400
Peroxidase activity	**k_{cat} (s^{-1})**	**K_M (mM)**	**k_{cat}/K_M ($s^{-1}M^{-1}$)**
WT KatG	0.63 ± 0.02	13 ± 1	48 ± 4
KatG S-Trp105	0.16 ± 0.01	51 ± 5	3 ± 0.3
KatG Y226F	4.20 ± 0.20	6.8 ± 1.1	620 ± 100

The appearance of this peptide, together with the absence of the canonical MYW CLPF, indicates that substitution of Trp105 with S-Trp redirects cofactor biogenesis away from crosslink formation toward an alternative, site-specific chemical modification. These HPLC and optical spectral signatures are consistent with modification at position 105—now bearing a S-Trp residue or an oxidized derivative—rather than nonspecific degradation or loss of the cofactor-forming region, setting the stage for molecular identification of the oxidative product within S-Trp105 KatG.

High-resolution mass spectrometry (HRMS) was used to further characterize this peptide. The calculated monoisotopic mass of 1165.48 Da corresponds to residues 103 – 112: ^{103}MAW*HGAGTYR^{112}. The observed mass of 1181.47 Da (Fig. 3B) represents a + 15.99 Da shift, consistent with monooxygenation. Collision-induced dissociation (CID) fragmentation of the doubly charged ion (*m/z* 591.75) localized the oxidation to the S-Trp105 residue. The 219.0332 Da mass difference between b2/b3 and y7/y8 fragment ions matched the calculated mass of [S-Trp]-O (219.0354 Da) (Fig. 3B, Supplementary table 1). These findings demonstrate that the genetically encoded S-Trp105 undergoes monooxygenation during expression.

Given this modification, we investigated the site of oxygen incorporation. While sulfoxide formation is a common outcome of oxidative products of heme or non-heme iron enzymes, including hydroxytryptophan[26–28], a benzothienopyrrole analogous to a pyrroloindole product[29], or 2-oxindole derivatives[30,31], were also considered (Fig. 4A). To determine whether oxygenation occurred at the sulfur atom of S-Trp105, FT-IR spectroscopy was used to probe for the

https://doi.org/10.1038/s41467-026-73579-y

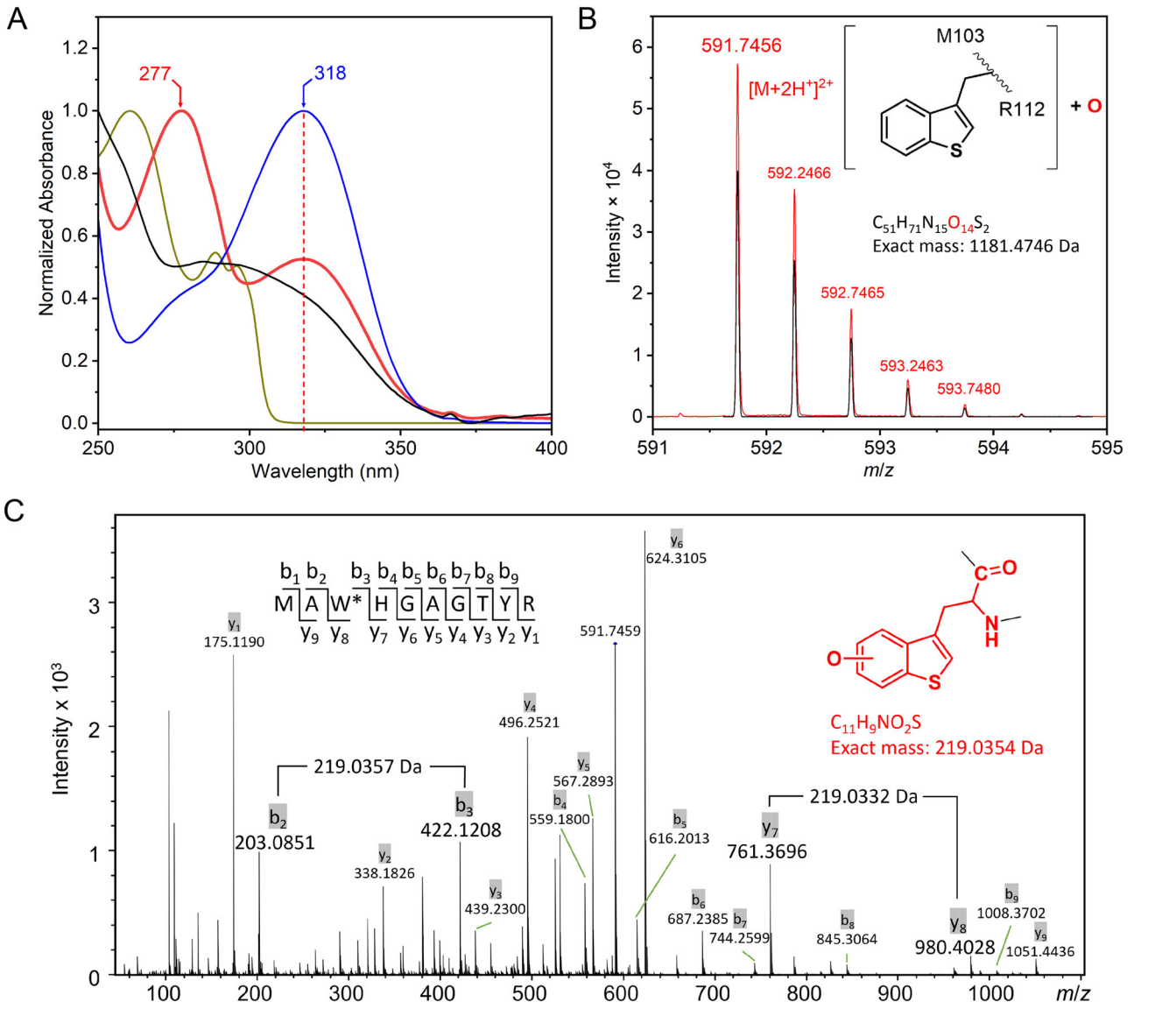

Fig. 3 | LC-MS analysis reveals autocatalytic oxidation of S-Trp in KatG. A UV-vis absorbance spectra of the peptide containing S-Trp105 (red), MYW-containing peptide from WT KatG (black), free S-Trp (dark yellow), and monooxygenated S-Trp standard (blue); all spectra are normalized to facilitate comparison. **B** High-resolution mass spectrum of the peptide bearing S-Trp105 (red), compared to the predicted isotopic distribution (black) **(C)** CID fragmentation spectrum of the S-Trp105 KatG-containing peptide; corresponding fragment ion assignments are provided in Supplementary Table 1.

diagnostic S = O stretching vibration in the 1000 − 1100 cm^{-1} region[32,33]. Control samples included WT KatG, sulfoxide-modified S-Trp (O = S-Trp) free amino acids in (*R*)- and (*S*)-configurations, and dimethyl sulfoxide (DMSO). The S-Trp105 KatG variant exhibits a pronounced absorption band at 1036 cm^{-1} that is absent in WT KatG (Fig. 4B). This feature closely matches the S = O stretching frequencies observed for free O = S-Trp and DMSO (~ 1041 cm^{-1}), providing strong spectroscopic evidence for site-specific sulfoxide formation at Trp105.

Chiroptical signatures reveal enantioselective formation of a chiral S-Trp sulfoxide

Having unambiguously established sulfur oxygenation at Trp105, we next asked whether this oxidation is stereoselective within the KatG active site. Although the benzothiophene ring of S-Trp is intrinsically planar, monooxygenation at the sulfur atom generates a stereogenic center, giving rise to two possible sulfoxide enantiomers. In a protein environment such as KatG, where the modified residue is conformationally constrained and oriented relative to the heme center, oxygen atom transfer is expected to occur preferentially from one face of the sulfur atom. Such spatial control provides a basis for enzymatic stereoselectivity, potentially yielding a dominant sulfoxide configuration rather than a racemic mixture.

To establish chiral reference standards, free O = S-Trp was synthesized following a published procedure[34], yielding two separable diastereomers, designated P1 and P2. The two isomers exhibited identical UV-vis spectra (Supplementary Fig. 5) and indistinguishable mass spectra (Supplementary Figs. 6, 7, and 9), while showing subtle but reproducible differences in their NMR profiles (Supplementary Figs. 8 and 10). Circular dichroism (CD) spectroscopy revealed mirror-image spectra for P1 and P2 (Fig. 4C), confirming that the two species share the same configuration at the α-carbon but differ in stereochemistry at the newly formed sulfur center (Fig. 4D).

To determine the stereochemical outcome of S-Trp oxidation within KatG, we next recorded the CD spectrum of the isolated

https://doi.org/10.1038/s41467-026-73579-y

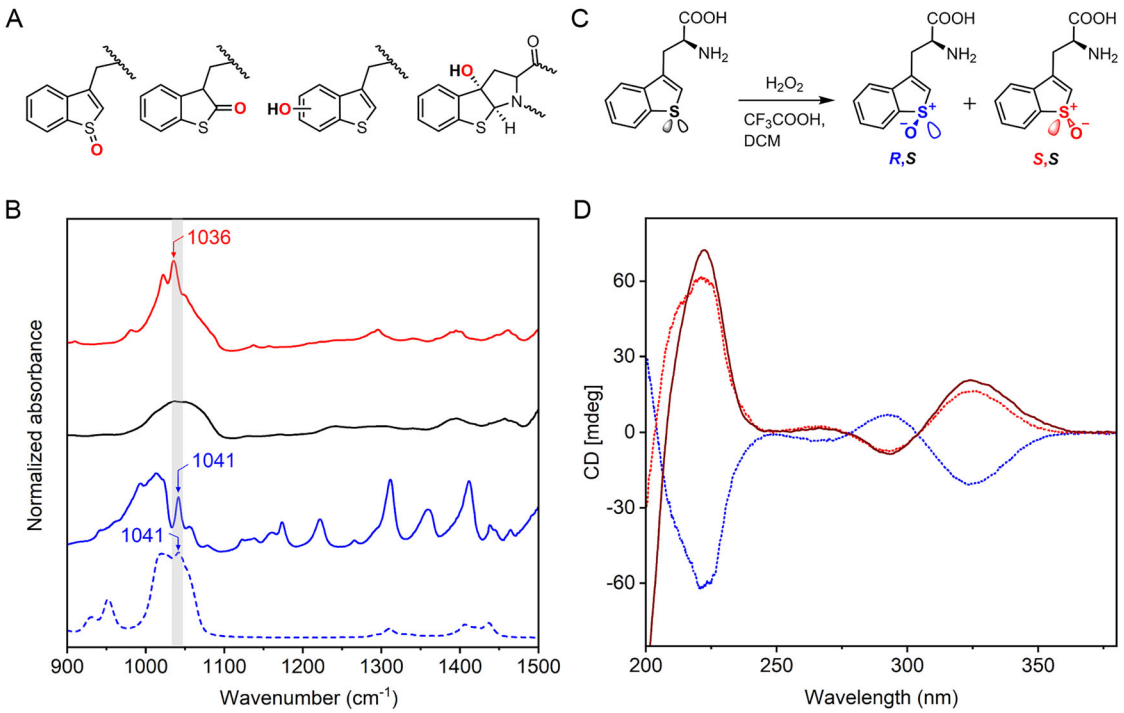

Fig. 4 | FT-IR and CD spectroscopies reveal regioselective sulfoxide formation and suggest a stereoselective S-oxygenation in KatG S-Trp105. A Chemical structures of potential monooxygenated and hydroxylated S-Trp species. **B** FT-IR spectra of lyophilized samples: WT KatG (black), KatG S-Trp105 (red), synthetic free O = S-Trp amino acid standard (solid blue), and DMSO (dashed blue). **C** Structures of two diastereomeric sulfoxides generated by non-enzymatic oxidation of S-Trp: (*R*,*S*) O = S-Trp and (*S*,*S*) O = S-Trp. **D** Circular dichroism spectra of free (*R*,*S*) (blue dots) and (*S*,*S*) (red dots) O = S-Trp amino acid standards, compared to the KatG peptide fragment that contains O = S-Trp105 (solid red trace). The peptide spectrum was smoothed using a Savitzky-Golay filter and normalized. Raw data are provided in Supplementary Fig. 11.

S-Trp–containing peptide. Strikingly, its CD profile closely matches that of synthetic diastereomer P2 (Fig. 4D; Supplementary Fig. 11), indicating that oxygenation occurs selectively at a specific face of the sulfur atom. This correspondence establishes that sulfoxidation in KatG is highly stereoselective rather than stochastic. Moreover, the observed CD signature closely resembles that reported for (1*R*)–3-methylbenzo[b]thiophene 1-oxide in the 200–400 nm region[35], supporting assignment of the oxidized residue in KatG as the (*S*)-configured sulfoxide, O = S-Trp105.

Cryo-EM reveals atomic-level structural redirection to an (S)-configured S-Trp sulfoxide

Previously reported MYW triad lacking variants apparently have large structural differences from the MYW-bearing or MYW-OOH-containing structures, and until now, no crystal structures of the MYW cofactor-free or partially crosslinked KatG mutants are available. The advance of cryo-EM technology has enabled the determination of a tryptophan mutant structure of Mtb KatG at 3.3 Å resolution, with the loop containing the MYW crosslink triad disordered, except for the introduced arginine[36]. Inspired by this prior work and through extensive optimization, we determined a high-resolution cryo-EM structure of full-length KatG bearing S-Trp at position 105 (Fig. 5). The structure was refined to 2.22 Å resolution (Supplementary Table 2, and Supplementary Fig. 12 for the cryo-EM workflow). The enzyme assembles as a D_2-symmetric tetramer, consistent with the oligomeric organization observed for WT KatG (Fig. 5A). The resulting density map is of sufficient quality to allow unambiguous visualization of the heme cofactor, surrounding conserved residues, and the modified S-Trp105 side chain within the active site (Fig. 5A).

The initial 2.29 Å raw map reconstruction exhibits a largely uniform local resolution distribution (Supplementary Fig. 13). Well-defined and continuous density is observed for the heme prosthetic group and key active-site residues, including Arg102, His106, Met252, and His267. The benzothiophene ring of S-Trp105 adopts an orientation closely matching that of Trp105 in WT KatG. Notably, additional electron density (Fig. 6A) is consistently observed at the sulfur atom of S-Trp105 in all four protomers, and the density is distinct from an unmodified Trp or S-Trp residue (Fig. 6B), a feature absent at all other tryptophan positions (Supplementary Fig. 14). This density is fully consistent with the formation of a sulfoxide (S = O) moiety, corroborating the FT-IR and optical spectroscopic analyses. Modeling of O = S-Trp105 using geometric restraints appropriate for an sp^3-hybridized sulfur atom (Supplementary Table 3) unambiguously favors the (*S*)-configuration at the sulfur center, with the sulfoxide oxygen oriented toward the heme iron. In contrast, an (*R*)-configured sulfoxide would direct the oxygen atom away from the heme and toward His106, a geometry incompatible with the observed density. This structural assignment independently confirms the stereochemical outcome inferred from CD spectroscopy.

Comparison with WT KatG structure reveals that substitution of Trp105 with S-Trp does not induce major rearrangements in the local active-site architecture. The side chain of O = S-Trp105 and neighboring residues (Arg102, His106, and Met252) remain closely aligned with their WT counterparts (Fig. 5A), indicating that the observed chemical redirection does not arise from global structural disruption. In contrast, pronounced differences are observed in the LL1 loop (Gly223–Ser240), which contains Tyr226, a constituent of the MYW cofactor.

In WT KatG, this loop is stabilized by covalent crosslinking and remains visible despite partial disorder[37]. In the S-Trp105 variant, however, a substantially expanded region of the LL1 loop (Trp197–Ser240) is unresolved in all four protomers (Fig. 5B), extending well beyond the disordered region observed in the WT enzyme. This loss of structural order is consistent with the absence of

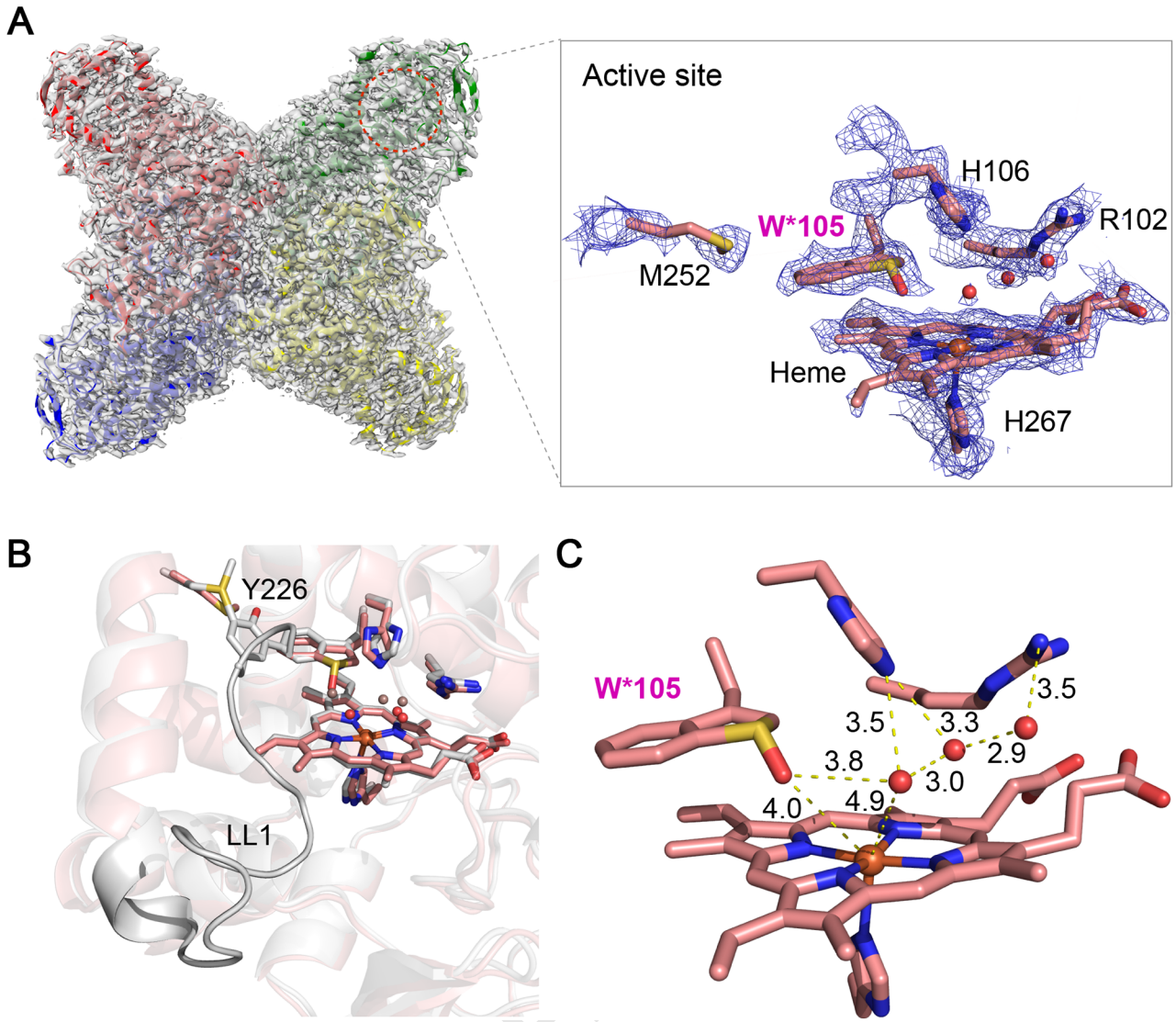

Fig. 5 | CryoEM structure of KatG S-Trp105 reveals asymmetric sulfoxide formation oriented toward the heme and absence of crosslinking. A Cryo-EM map and atomic model of tetrameric KatG S-Trp105 at 2.22 Å resolution (density modified; raw map resolution 2.29 Å); each protomer is shown in a distinct color (PDB entry: 9O6A)[58]. **B** Close-up view of the enzyme active site showing the cryo-EM density and model fit. The sulfoxide adopts an (*S*) configuration, consistent with the observed asymmetric density at S-Trp105. **C** Structural overlay of KatG S-Trp105 (salmon, this study) and WT KatG (gray, PDB: 7JZ6), showing an RMSD of 0.440 Å across 611 aligned Cα atoms. The LL1 loop is partially ordered in the WT structure and unresolved in the S-Trp105 variant. **D** Zoomed-in view of the heme active site and distal pocket, highlighting key residues and interatomic distances (in Å).

MYW crosslink formation and aligns with the spectroscopic, mass spectrometric, and functional data.

Taken together, the cryo-EM structure of KatG S-Trp105 provides direct, atomic-level evidence that a single-atom NH → S substitution redirects oxidative chemistry at the active site from radical-mediated crosslinking to stereoselective sulfoxidation (Fig. 6). The proximity of the sulfoxide oxygen to the heme iron (~4.0 Å; Fig. 5C) offers a structural basis for the altered electronic coupling and the pronounced suppression of catalase and peroxidase activities observed for this variant.

Two-electron oxygenation of S-Trp105 requires heme-dependent peroxide activation

To probe the mechanism underlying S-Trp105 oxidation, we generated a heme-deficient form of KatG S-Trp105 by culturing cells in iron-depleted medium. The resulting protein exhibited markedly reduced heme incorporation, as indicated by a low R_z value (0.080, compared to 0.361 for WT KatG), where the R_z value is defined as the ratio of the absorbance of the Soret band to the absorbance of the protein peak. Subsequent in vitro heme reconstitution yielded reconstituted EcKatG S-Trp105 (^{R}EcKatG S-Trp105) with a substantially increased R_z value of 0.645 (Supplementary Fig. 15), confirming restoration of an intact heme center.

To determine whether S-Trp105 oxygenation requires heme-mediated catalysis, both the heme-deficient and reconstituted S-Trp105 variants were treated with oxidants (5 equivalents of H_2O_2 or peracetic acid), followed by tryptic digestion and HPLC analysis. The formation of the oxidized S-Trp105 species, monitored by characteristic absorbance at 330 and 318 nm, was observed exclusively in the reconstituted enzyme (Fig. 7). No sulfoxide formation was detected in the heme-deficient protein under identical conditions. High-resolution mass spectrometry and CID analysis of the oxidized peptide (Supplementary Fig. 16, Supplementary Table 1) confirmed that it is identical to

https://doi.org/10.1038/s41467-026-73579-y

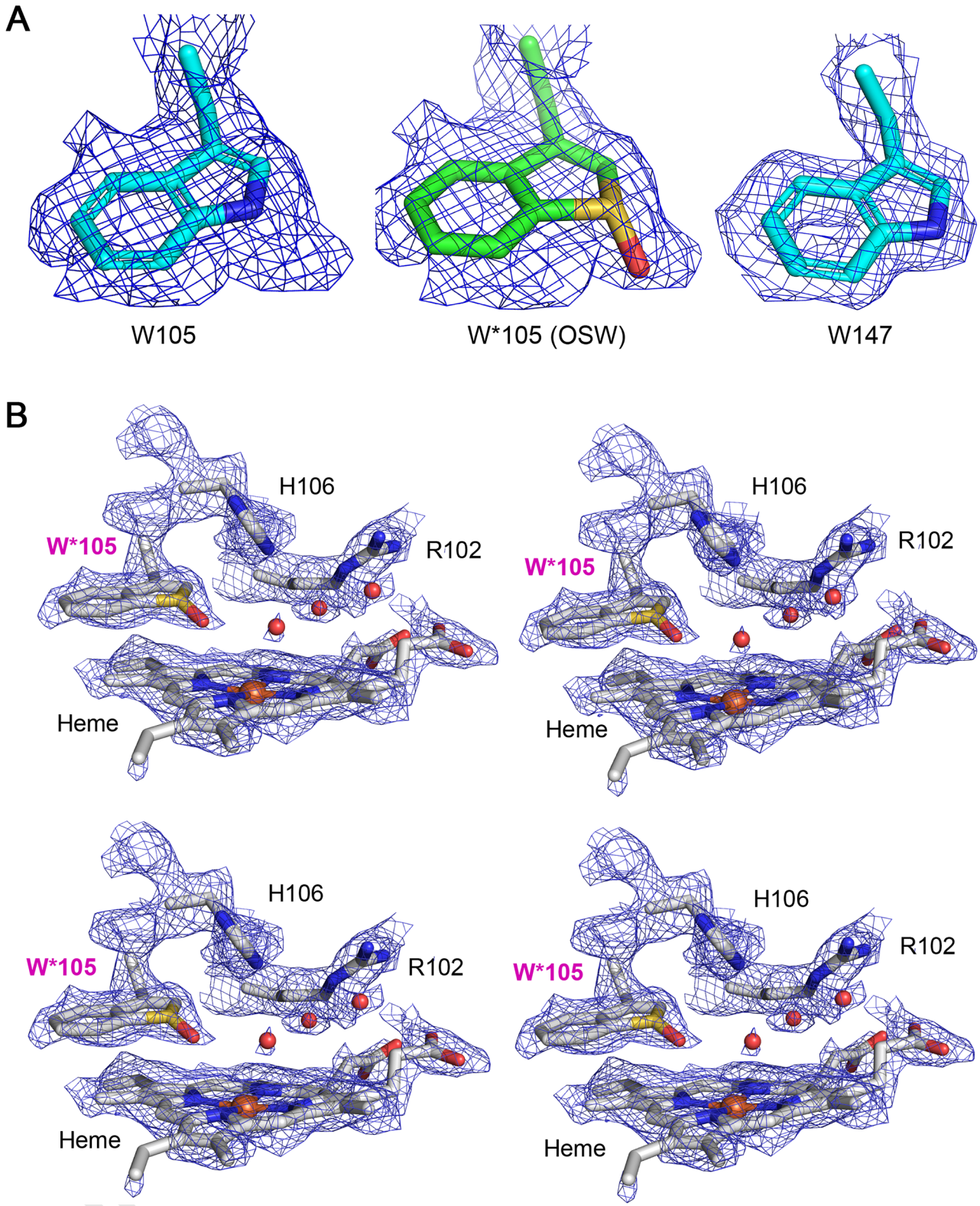

Fig. 6 | Stereogenic center of O = S-Trp105 in the cryo-EM structure of the engineered KatG variant. A Comparison of density map and model fitting on unmodified Trp, monooxygenated S-Trp (W*, molecular code in the 3D structure: OSW), and Trp147. Supplementary Fig. 14 shows the comparison of O = S-Trp electron density with all other Trp residues in the same KatG structure. **B** The (*S*)-configured aromatic sulfur atom-centered configuration is uniformly observed in all four chains of the asymmetric unit. The cryo-EM density map is contoured at 4.5 σ (ChimeraX).

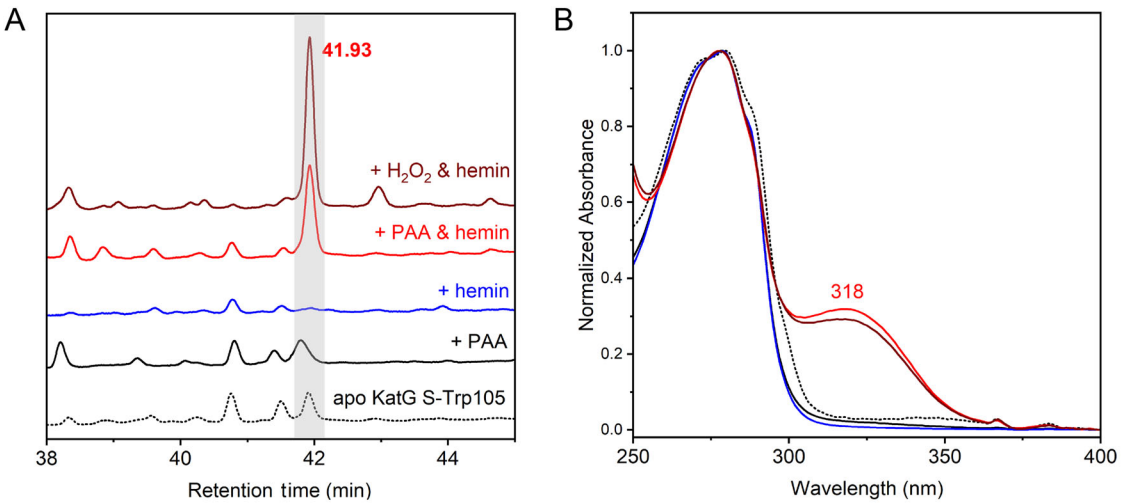

Fig. 7 | Heme and peroxide are required for S-Trp105 oxidation. A HPLC profiles of trypsin-digested samples: apo-KatG S-Trp105 treated with five equivalents of peracetic acid (black solid line), untreated apo-KatG S-Trp105 (black dashed), heme-reconstituted KatG S-Trp105 without oxidant (blue), and heme-reconstituted protein treated with peracetic acid (red) or H_2O_2 (magenta). **B** UV-vis spectra of HPLC fractions (retention time = 41.93 min). Only peptides from heme-reconstituted protein oxidized with peroxide exhibit the 318 nm absorbance peak characteristic of O = S-Trp.

the O = S-Trp-containing peptide detected in the as-isolated S-Trp105 KatG (Fig. 3B).

These results demonstrate that S-Trp105 monooxygenation is strictly dependent on the presence of a functional heme center and an exogenous oxidant, establishing that sulfoxide formation is an active-site-mediated process rather than a nonspecific chemical modification. Together with the spectroscopic and structural data, these findings support a heme-dependent two-electron oxygen-atom transfer mechanism that autocatalytically converts the genetically incorporated S-Trp residue into a chiral sulfoxide in the mature enzyme. This pathway contrasts sharply with the radical-mediated chemistry of native Trp105 and underscores how a single-atom substitution redirects KatG reactivity.

Discussion

Hydrogen atom abstraction (HAT) and transfer are fundamental to enzymatic redox catalysis, yet experimentally disentangling residue-specific contributions within complex active sites remains a long-standing challenge. In catalase–peroxidase (KatG), a heme-mediated HAT from the indole N–H of the cofactor-bearing Trp residue has long been proposed as the initiating step for both MYW cofactor biogenesis and catalase function[5,9,11,16,38–40]. However, direct experimental interrogation of the role of this specific proton has remained elusive. In this study, we show that substituting the indole N–H with sulfur at this single cofactor-forming position is sufficient to reroute the oxidative chemistry of KatG, demonstrating that the indole N–H is not merely permissive but obligate for enforcing the native radical pathway. By replacing Trp105 with thiotryptophan via genetic code expansion, we uncover an unexpected, site-specific, and stereoselective sulfoxidation catalyzed by the KatG heme center. This chemical redirection diverts oxidative flux away from the canonical one-electron, radical-mediated pathway responsible for MYW cofactor formation and instead reveals a two-electron oxygen-atom transfer process that is normally inaccessible in the native enzyme (Table 2).

The engineered PylRS used in this study is specific in that it excludes the native Trp, indicating that it has achieved a high level of stereoelectronic complementarity for the sulfur atom. The PylRS active site is precisely tuned to the distinct bond lengths and polarizability of its cognate ncAA (S-Trp), highlighting the single-atom precision of this approach. The observed sulfoxidation is remarkable in several respects. First, it occurs on an internally encoded residue rather than an external substrate, demonstrating that KatG can catalyze monooxygenase-like chemistry within its own active site. Second, the reaction proceeds with regio- and stereo-selectivity, yielding the (*S*)-configured sulfoxide. Third, this chemistry is revealed not by altering the protein fold or active-site architecture, but by a minimal NH → S substitution that preserves aromaticity while fundamentally changing redox behavior. Together, these features indicate that KatG possesses an alternative chemical capability that is normally constrained by the chemical identity of Trp105.

The MYW crosslinking process has been hypothesized to begin with an HAT step on the indole N-H and three other HAT steps in two rounds of H_2O_2 oxidation (Fig. 8A, and for details see Supplementary Fig. 1)[8,9,16,17]. Experimental evidence for this biosynthetic sequence is difficult to obtain. Mechanistically, our data support a model in which removal of the indole N-H group blocks the initial HAT for MYW biogenesis and thereby redirects oxidation to a two-electron oxygen atom transfer (OAT) at the aromatic sulfur atom (Fig. 8B). The most plausible oxidant is Compound I (cpd I, i.e., ferryl and porphyrin π-cation radical). The strict dependence on an intact heme center and peroxide activation, together with the stereochemical outcome, argues against a radical-based mechanism and instead favors a constrained Fe–O···S transition state that enforces facial selectivity (Fig. 8B). Cryo-EM observation of the sulfoxide oxygen oriented toward the heme iron provides a structural rationale for both the stereoselectivity and the pronounced perturbation of catalytic activity.

KatG's ability to promote this transformation contrasts sharply with related heme peroxidases such as cytochrome *c* peroxidase (CcP) and ascorbate peroxidase (APX), where analogous active-site tryptophan residues are present and remain unmodified during catalysis[41,42]. This distinction likely reflects differences in oxidant reactivity and active-site dynamics: KatG favors highly reactive ferryl intermediates capable of driving oxygen-atom transfer, whereas CcP stabilizes a long-lived Compound ES (ferryl and an adjacent amino acid radical) state[43]. Consistent with this view, S-Trp substitution in CcP does not result in sulfoxidation despite the closer proximity of the sulfur atom to the heme center[24]. Thus, KatG's distal pocket appears poised to enable controlled, enzyme-mediated aromatic sulfur oxidation.

An additional advance of this study is the use of high-resolution cryo-electron microscopy to visualize, at atomic detail, a site-specific

Table 2 | Single-atom substitution redirects catalytic pathways in KatG

Native tryptophan (N–H)	Thio-tryptophan (S)
Radical-initiated HAT pathway	HAT pathway inaccessible
Formation of Trp-centered radical (Trp-N˙)	Two-electron aromatic S-oxygenation
MYW crosslink formation	Monooxygenase-like modification of an internal residue
Canonical catalase and peroxidase activities	Suppressed catalase activity and attenuated peroxidase activity

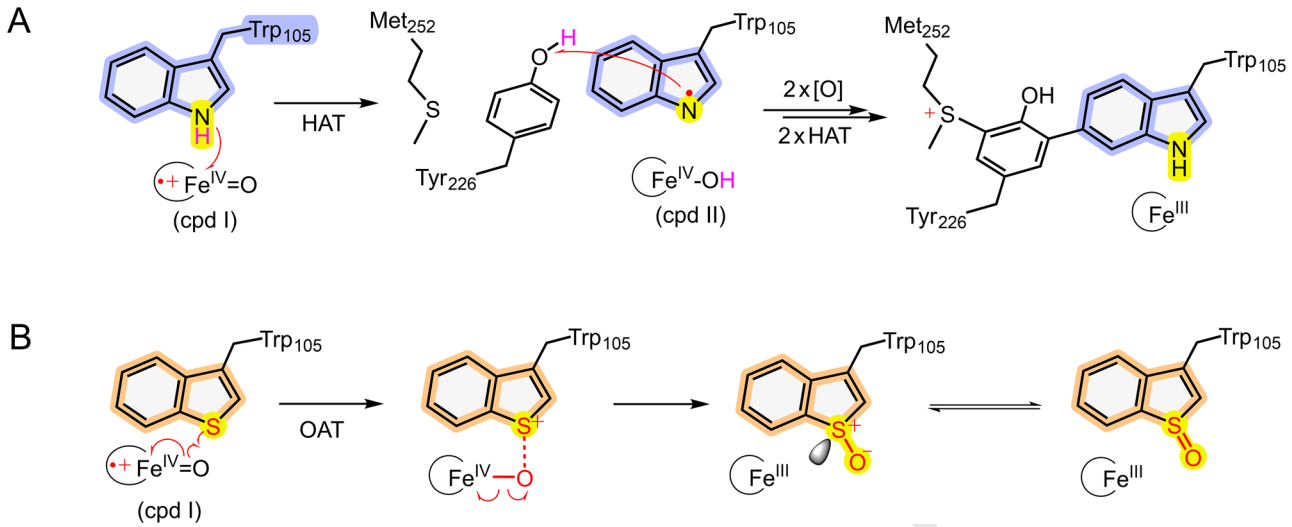

Fig. 8 | Single-atom substitution redirects KatG reactivity from one-electron, radical-mediated hydrogen atom transfer (HAT) chemistry for cofactor biogenesis to stereoselective sulfoxidation via a two-electron oxygen-atom transfer (OAT). Native pathway (Path **A**) proceeds via a radical-mediated mechanism initiated by an obligatory HAT from the indole N-H group to cpd I. This leads to the autocatalytic assembly of the Met–Tyr–Trp (MYW) crosslinked cofactor (for detailed arrow pushing of the biogenesis steps, see Supplementary Fig. 1). S-Trp variant (Path **B**) circumvents the radical path and instead facilitates a two-electron OAT. This direct oxidation, indicated by detailed arrow pushing, proceeds through a constrained ferryl (Fe^{IV}) transition state. This interaction enhances facial selectivity, ultimately yielding the (*S*)-configured thiotryptophan sulfoxide while returning the heme to the ferric (Fe^{III}) state.

post-translational modification of a genetically encoded noncanonical amino acid within an enzyme active site, even though this technology has previously been used to determine KatG structures[36,37]. The cryo-EM structure reported in this study reveals how local chemical modification propagates to disrupt MYW crosslink formation without inducing large-scale structural rearrangements. This represents a direct structural observation of enzyme-catalyzed sulfoxidation of an internally incorporated noncanonical residue.

More broadly, this work illustrates how ncAA substitution can be used not merely to test functional necessity but to actively redirect enzymatic reaction pathways and expose hidden catalytic capabilities. The distinct FT-IR and CD signatures of sulfoxide formation provide powerful spectroscopic handles for tracking regio- and stereochemical outcomes, suggesting that S-Trp may serve as a general probe for interrogating tryptophan-mediated redox chemistry. It is worth mentioning that genetic substitution of S-Trp into proteins is a recently developed technique, with prior efforts mainly aimed at probing the hydrogen-bonding roles of indole nitrogen in enzymes such as CcP, deubiquitinase, and thioredoxin[23,24,44]. Given the prevalence of indole and tryptophan in flavin- and metal–dependent oxidation systems, this strategy may find broad application in dissecting and reprogramming oxidative transformations across enzyme families.

Our results reveal the alternative chemical capability of the KatG active site and show how the chemical identity of the indole N–H proton channels reactivity into the native radical pathway. Active-site tryptophan residues in heme peroxidases are intrinsically reactive: although residues such as Trp51 in CcP and the proximal Trp in APX often remain unmodified, perturbations in the distal pocket can promote one-electron oxidation to give protein-based radicals or covalent heme-protein linkages. Examples, including the autocatalytic Trp51–Tyr52 crosslink in CcP mutants and the Tyr-heme/Trp-heme adducts observed in APX after peroxide treatment, illustrate that these residues are poised for oxidative transformation[45–47]. By contrast, the redirection of KatG chemistry to a site-specific, two-electron sulfoxidation of an internally encoded noncanonical residue represents a mechanistic departure from the one-electron pathways described above (Fig. 8). Moreover, peroxidase-catalyzed enantioselective oxidations of free sulfides have been reported for various peroxidases, such as haloperoxidases, lignin peroxidase, and engineered dye-decolorizing peroxidases (DyPs)[48–54], and human indoleamine 2,3-dioxygenase (IDO) has been shown to perform monooxygenation on free S-Trp[55]. However, the endogenous aromatic sulfide modification observed in S-Trp KatG is distinct from these precedents. Rather than acting on an external substrate, the stereoselective sulfoxidation occurs within the KatG scaffold itself, illustrating how a single-atom substitution can reprogram the enzyme's internal maturation trajectory.

In summary, replacing a single heteroatom at Trp105 transforms KatG from a radical-based cofactor-forming enzyme into one that catalyzes stereoselective aromatic sulfoxidation. This atomic-level intervention reveals how enzyme function can be switched not by altering structure, but by redirecting chemistry—highlighting a powerful paradigm for probing and reengineering complex enzymatic redox processes.

Methods

Materials

The primers were purchased from Integrated DNA Technologies (IDT). All chemical reagents were purchased from Sigma-Aldrich or Thermo Fisher Scientific and were of reagent grade or higher and used as

received. DNA manipulations in Escherichia coli (E. coli) were carried out according to standard procedures. Ampicillin (100 μg/mL) and chloramphenicol (30 μg/mL) were used as antibiotics to select recombinant strains.

Generation of site-specific S-Trp-encoded KatG variant

EcKatG was chosen for this study due to its significantly higher protein expression efficiency compared to other available KatG expression systems. The katG gene was amplified from E. coli (K-12) genomic DNA and cloned into the pET-20b(+) vector containing a C-terminal six-histidine tag, which was developed in the Goodwin laboratory at Auburn University, Alabama, USA[25]. The resulting pET-20b(+)-EcKatG plasmid was used to transform an E. coli protein expression host (BL21 [DE3]), and transformants were selected based on their ampicillin resistance (100 μg/ml ampicillin). We generated W105TAG KatG mutant using the primers provided below:

5′- GGCCTAGCACGGCGCGGGGACTTACCGTTCAATCG −3′ and 5′-GCCGTGCTAGGCCATACGAATAAACAG ACCGGCG-3′. Polymerase chain reaction (PCR) for generating the variants was performed using Phusion High-Fidelity polymerase with GC-buffer (Thermo Fisher Scientific). The PCR products were treated with DpnI to eliminate the template. Subsequently, E. coli DH10B was transformed with the DpnI-treated PCR products using a standard heat-shock procedure. Candidate plasmids were analyzed for complete sequence by Eurofins Genomics to verify the intended alterations. The pET-20b(+)-EcKatG_W105TAG plasmid was co-transformed into E. coli BL21(DE3) with the plasmid expressing a previously reported orthogonal tRNA/aaRS pair for S-Trp (pEVOL_PylRS_S-Trp plasmid)[24], and the cells were plated onto an LB agar plate containing 100 μg/ml ampicillin and 30 μg/ml chloramphenicol.

Protein expression and purification

The expression plasmid construct of EcKatG S-Trp105 was transformed into E. coli BL21(DE3), and transformants were selected based on resistance to chloramphenicol/ampicillin for EcKatG S-Trp105 expression. The bacteria were grown in an LB broth medium containing ampicillin (100 μg/ml) and chloramphenicol (30 μg/ml) in a baffled flask at 37 °C, 220 rpm. Arabinose, δ-aminolevulinic acid, and ferrous ammonium sulfate were added to a final concentration of 10 mM, 200 μM, and 25 μM, respectively. When the optical density at 600 nm (OD_{600}) reached 0.4, isopropyl β-D-1-thiogalactopyranoside (IPTG) and S-Trp were added to a final concentration of 0.5 mM and 1 mM, respectively. After 12 − 14 h of incubation at 32 °C, 180 rpm, the cells were harvested and frozen at −80 °C for further use.

KatG S-Trp105 was purified by a fast protein liquid chromatography (FPLC) system. Cell pellets were resuspended in 100 mM sodium phosphate (NaPi) buffer (pH 7.0) with ~0.1 mM phenylmethylsulfonyl fluoride (PMSF) and then lysed by sonication. The supernatant was recovered upon centrifugation (34,000 × *g* for 40 min) at 4 °C and then applied to Ni-NTA agarose beads. After loading, the Ni-NTA agarose beads were washed with 2 column volumes of washing buffer (100 mM NaPi, 20 mM imidazole, pH 7.0). The His_6-tagged protein was eluted with elution buffer (100 mM NaPi, 500 mM imidazole, pH 7.0). The eluted KatG S-Trp105 protein was further purified by a Superdex 200 (Cytiva) gel-filtration column (16/600) with 50 mM NaPi buffer (pH 7.0) as the mobile phase. The purified protein was either concentrated by ultrafiltration to the required concentration for subsequent experiments or stored in 50 mM NaPi, 5% glycerol buffer (pH 7.0) at −80 °C. The concentration of active heme protein was determined using the standard pyridine hemochromagen assay.

Expression of apo-EcKatG S-Trp105 and heme-reconstitution

As previously described, the apo-EcKatG S-Trp (heme-free) was prepared by cell culture in iron-free medium[9]. All glassware was rinsed with 1 M HNO_3 solution followed by deionized water (Millipore) before use. The iron-free medium was prepared by dissolving 10 g of casamino acids, 5 g of yeast extract, and 10 g of sodium chloride in 1 L of deionized water. Chelex 100 (30 g) resin was added to the medium and stirred for 2 h to remove trace metals. After filtration, the medium was transferred to a 2 L glass baffled flask and autoclaved. Supplemental ions and solutions, including 2 mM $MgSO_4$, 0.1 mM $CaCl_2$, vitamin mix (10 ml of a 100 mL stock: 10 mg each of riboflavin, niacinamide, pyridoxine monohydrate, and thiamine in 100 mL of H_2O), and iron-free trace metals mix (10 mL of a 100 mL stock: 0.5 g of EDTA, 5 mg each of $ZnCl_2$, $CuCl_2$, $CoCl_2$, and H_3BO_3, 160 mg of $MnCl_2$, 50 mg of $NiSO_4$, 100 ml of H_2O), were added to the medium. The cell culture method was the same as the KatG S-Trp105, except that δ-aminolevulinic acid and ferrous ammonium sulfate were not added. The protein purification method was the same as for KatG S-Trp105.

Heme reconstitution for apo-EcKatG S-Trp105 was performed in 50 mM HEPES buffer (pH 8). A 5 mM stock solution of hemin was prepared by dissolving hemin into 50 mM NaOH solution. Hemin (1.5 molar equivalents relative to the protein) was added dropwise to the protein solution under stirring. The mixture was stirred at 4 °C for 2 h to allow complete hemin binding. The mixture was centrifuged at 20,000 × *g* for 5 min to remove any precipitated hemin and protein.

Enzymatic activity and kinetics assay

Catalase activity was evaluated by measuring the O_2 production rate using Oxygraph (Hansatech Pentney, Norfolk, England). The instrument was calibrated using sodium dithionite solution and air-saturated water. The reaction was initiated by adding 5 − 500 nM KatG enzyme to 0.25 − 25 mM H_2O_2 solution. All activity assays were carried out at 22 °C under 100 rpm stirring in 50 mM NaPi buffer (pH 7.0). The oxygen production speed was recorded and fitted with a hyperbolic curve using Origin software. Peroxidase activity was evaluated by monitoring the production rate of the 2,2′-azino-bis(3-ethylbenzothiazoline-6-sulfonic acid) (ABTS) radical ($\varepsilon_{417} = 34.7\ mM^{-1}cm^{-1}$) using a Thermo Evolution Pro UV-vis spectrophotometer. The reaction was initiated by adding 5 to 500 nM KatG enzyme to 1 mM ABTS and 0.5 to 30 mM tert-butyl hydroperoxide (tBuOOH). All assays were carried out at 22 °C using 50 mM NaPi buffer (pH 7.0). Activity assays were performed in triplicate (three independent replicates). Data are presented as mean ± SD, and individual replicate values are shown as overlaid points on each plot.

Trypsin digestion of protein and HPLC assay

Protein was diluted to a 2 mg/mL stock solution in 50 mM NH_4HCO_3 buffer (pH 8.5). MS grade trypsin protease (Fisher Scientific) was dissolved in the same NH_4HCO_3 buffer to a concentration of 1 mg/mL. A protein stock (100 μL) was mixed with 4 μL trypsin solution, leading to a 50:1 w/w ratio. The mixture was incubated at 37 °C for 48 h to ensure complete digestion. The digested protein samples were analyzed by SDS-PAGE to verify complete digestion. For the preparation and digestion of the ^{R}EcKatG S-Trp105 sample, 50 mM HEPES buffer (pH 8.0) was used for digestion and heme reconstitution.

The digested protein was centrifuged at 20,000 × *g* for 5 min to remove any precipitate. A 100 μL sample was injected into an Inertsil ODS-3 HPLC column, 3 μm, 250 ×4.6 mm (GL Sciences) using an UltiMate 3000 HPLC (Thermo Scientific). The separation was performed using a linear gradient of buffer B (0.1% trifluoroacetic acid in acetonitrile) in buffer A (0.1% trifluoroacetic acid in water) from 0 − 60% over 2 h at a flow rate of 0.5 mL/min. Fractions with absorbance at 330 nm were collected and stored for MS analysis.

Protein mass spectrometry

High-resolution electrospray ionization mass spectra (ESI-MS) were acquired using a maXis plus quadrupole-time-of-flight mass spectrometer (Bruker Daltonics) operated in positive-ion mode. Samples were

directly infused from HPLC fractions into the ESI source using a syringe pump at a constant flow rate of 3 µL/min. Key source parameters were as follows: capillary voltage, 3500 V; nebulizer gas pressure, 0.4 bar; dry gas flow rate, 4.0 L/min; source temperature, 200 °C. CID was performed with an average collision energy of approximately 25 eV. Mass spectra were averages of 1-minute scans collected at a rate of 1 scan per second in the mass-to-charge ratio (m/z) range of 50 − 1500. Compass Data Analysis software version 4.3 (Bruker Daltonics) was used for all mass spectral data processing. Theoretical masses for b- and y-type fragment ions were calculated using the MS-Product utility of ProteinProspector (https://prospector.ucsf.edu/prospector/mshome.htm).

Synthesis and separation of S-monooxygenated S-Trp (O = S-Trp)

Free O = S-Trp amino acid was synthesized following a modified published method[34]. Thiotryptophan (3-benzothienyl-L-alanine, or S-Trp) (221 mg, 1.0 equiv), 2 mL of dichloromethane, and 2 mL of trifluoroacetic acid were added to a round-bottom flask and cooled to 0 °C in an ice bath. An aqueous solution of H_2O_2 (0.88 mL, 30 wt%, 1.2 equiv) was added dropwise to the mixture. The flask was removed from the ice bath, and the mixture was stirred at room temperature for 1 h. The reaction was quenched with saturated $NaHCO_3$ solution and transferred to a separatory funnel. The organic layer was evaporated using a rotary evaporator, and the resulting solid was redissolved in water, combined with the aqueous layer, and lyophilized to yield an off-white powder. The solid powder was redissolved in 0.1% formic acid (FA) solution, filtered through a 0.22 µm filter, and separated by HPLC. For analytical HPLC, a 50 µL sample was injected onto an Inertsil ODS-3 HPLC column (3 µm, 100 × 4.6 mm, GL Sciences) using an UltiMate 3000 HPLC system (Thermo Scientific). Separation was achieved using an isocratic mobile phase of 30% acetonitrile, 0.1% FA, and 69.9% H_2O at a flow rate of 0.5 mL/min. For preparative HPLC separation, a 500 µL sample was injected onto a Hypersil PREP HS C18 column (5 µm, 250 × 10 mm, Thermo Scientific) using a preparative UltiMate 3000 HPLC system (Thermo Scientific). Fractions were separated using an isocratic mobile phase of 30% acetonitrile, 0.1% FA, and 69.9% H_2O at a flow rate of 3.5 mL/min. The collected fractions were lyophilized to a white powder and stored at −80 °C for future use.

Optical and circular dichroism (CD) spectroscopies

UV-vis spectra were recorded at 22 °C in 50 mM NaPi buffer (pH 7.0), using a Thermo Evolution Pro UV-vis spectrophotometer. Fourier-transform infrared spectroscopy (FT-IR) spectra were collected using a Nicolet Nexus 470 FT-IR spectrometer with an ATR module. The spectra were acquired using lyophilized protein and commercially available chemicals. Circular dichroism (CD) spectra were recorded at 22 °C in deionized water using a Jasco J-1100 CD spectrometer under a continuous N_2 purge with a cuvette path length of 1 mm.

Electron paramagnetic resonance (EPR) spectroscopy

Q6

X-band continuous-wave EPR spectra were recorded on a Bruker E560 spectrometer equipped with a cryogen-free 4 K temperature system and an SHQE high-Q resonator, as described previously[56,57]. The measurements were performed at 9.37 GHz with 100 kHz modulation frequency, 1 mW microwave power, 0.6 mT modulation amplitude at 10 K, and an average of four scans for each spectrum. The EPR samples were 80 µM KatG protein (determined by heme concentration) in 50 mM NaPi buffer (pH 7.0) and were frozen in liquid nitrogen for storage.

Cryo-EM sample preparation and data collection

Cryo-EM samples were prepared applying KatG S-Trp105 to grids at the Stanford-SLAC CryoEM Center (S^2C^2). KatG S-Trp105 protein samples were diluted to 1.5 µM in a 50 mM Tris-HCl and 50 mM NaCl buffer at pH 8.0. Grids were prepared using glow-discharged holey carbon grids (Quantifoil R2/1 Cu 200 mesh) and plunged into liquid ethane using a Thermo Fisher Scientific Vitrobot (Mk IV) cryo-plunger. Prior to sample application, grids were glow-discharged (PELCO easiGlow) at 15 mA for 30 s at 0.26 mbar residual atmosphere. A 3 µL aliquot of the sample was applied to each grid and blotted for 3 s under environmental chamber conditions of 100% humidity and 4 °C.

Cryo-EM data were collected at S^2C^2 using an Alpha Titan Krios G3i transmission electron microscope (TEM) (Thermo Fisher Scientific) operating at 300 keV, equipped with a Falcon 4i electron detector and a Selectris X energy filter (10 eV silt). Images were collected at a magnification of 130,000×, resulting in a pixel size of 0.954 Å per pixel, with an electron exposure of ~50 $e^-/Å^2$ at a dose rate of ~1.14 e^- per frame. The objective-lens defocus range was set between −1.0 and −2.0 µm.

Cryo-EM data processing, Model building and refinement

Cryo-EM data processing was performed using cryoSPARC (Version 4.5.3). A total of 18,517 movies were imported. Following motion correction and contrast transfer function (CTF) estimation, 15,512 micrographs were retained for further analysis. Initial particle picking was performed using the blob picker with a particle diameter range of 100 − 220 Å. Particles were extracted from these micrographs with a box size of 240 pixels (downsized to 60 pixels by 4× binning), yielding 7,762,366 particles. These particles underwent three rounds of 2D classification, resulting in 2,821,979 particles. An ab initio reconstruction was then performed, sorting these particles into three volume classes.

To enrich rare-view particles, the particles from the best volume class were used as templates for template picking. This process generated 6,955,031 particles, which were then subjected to 2D classification, selecting 731,599 rare-view particles. These rare-view particles were combined with the previously retained particle set, resulting in a merged dataset of 3,060,258 particles. This combined set underwent heterogeneous refinement, and particle orientation was rebalanced, reducing the dataset to 884,126 particles from the best volume class. These particles were re-extracted with a box size of 240 pixels (unbinned) and further refined through sequential steps of homogeneous, non-uniform, and CTF refinement to produce the final reconstruction at 2.29 Å resolution.

The raw map from CryoSPARC was improved using the resolve_cryo_em job in Phenix (version 2.0rc1-5599), resulting in a density-modified map at 2.22 Å resolution. The initial template was from PDB 7JZ6 and docked into the map using phenix.dock_in_map. The model was refined using Coot (version 0.9.8.1) and phenix.real_space_refinement. The restraint of O = S-Trp was generated based on the geometry of sp^3 hybridization and reference small-molecule structures (CCDC number 2236439). Statistics associated with data collection, 3D reconstruction, and model refinement are included in Supplementary Tables 2, and 3, and Supplementary Fig. 12.

Reporting summary

Further information on research design is available in the Nature Portfolio Reporting Summary linked to this article.

Data availability

All data described in this study are included in the manuscript and the accompanying Supporting Information. The protein mass spectrometry datasets associated with Fig. 3 and Supplementary fig. 16 have been deposited in the ProteomeXchange Consortium via the PRIDE partner repository with the dataset identifiers PXD078006 for Fig. 2C and PXD078069 for Supplementary fig. 16, respectively. The cryo-EM raw data generated in this study have been deposited in the Electron Microscopy Data Bank (EMDB) under accession number EMD-70168 [https://www.ebi.ac.uk/emdb/EMD-70168], and the corresponding 3D

coordinates have been deposited in the Protein Data Bank (PDB) under entry code 9O6A[58]. The PDB code of the previously published structure used in this study is 7JZ6. Source Data are provided as a Source Data file. Source data are provided with this paper.

References

1. Zámocká, M. et al. High conformational stability of secreted eukaryotic catalase-peroxidases: answers from first crystal structure and unfolding studies. *J. Biol. Chem.* **287**, 32254–32262 (2012).
2. Chouchane, S., Girotto, S., Yu, S. & Magliozzo, R. S. Identification and characterization of tyrosyl radical formation in *Mycobacterium tuberculosis* catalase-peroxidase (KatG). *J. Biol. Chem.* **277**, 42633–42638 (2002).
3. Regelsberger, G. et al. Effect of distal cavity mutations on the formation of compound I in catalase-peroxidases. *J. Biol. Chem.* **275**, 22854–22861 (2000).
4. Zámocký, M., Gasselhuber, B., Furtmüller, P. G. & Obinger, C. Molecular evolution of hydrogen peroxide degrading enzymes. *Arch. Biochem Biophys.* **525**, 131–144 (2012).
5. Zhao, X. et al. A radical on the Met-Tyr-Trp modification required for catalase activity in catalase-peroxidase is established by isotopic labeling and site-directed mutagenesis. *J. Am. Chem. Soc.* **132**, 8268–8269 (2010).
6. Loewen, P. C., Carpena, X., Vidossich, P., Fita, I. & Rovira, C. An ionizable active-site tryptophan imparts catalase activity to a peroxidase core. *J. Am. Chem. Soc.* **136**, 7249–7252 (2014).
7. Graciano, A. & Liu, A. Protein-derived cofactors: chemical innovations expanding enzyme catalysis. *Chem. Soc. Rev.* **54**, 4502–4530 (2025).
8. Ghiladi, R. A., Medzihradszky, K. F. & Ortiz de Montellano, P. R. Role of the Met-Tyr-Trp cross-link in *Mycobacterium tuberculosis* catalase-peroxidase (KatG) as revealed by KatG (M255I). *Biochemistry* **44**, 15093–15105 (2005).
9. Ghiladi, R. A., Knudsen, G. M., Medzihradszky, K. F. & Ortiz de Montellano, P. R. The Met-Tyr-Trp cross-link in *Mycobacterium tuberculosis* catalase-peroxidase (KatG): Autocatalytic formation and effect on enzyme catalysis and spectroscopic properties. *J. Biol. Chem.* **280**, 22651–22663 (2005).
10. Zamocky, M. et al. High conformational stability of secreted eukaryotic catalase-peroxidases. *J. Biol. Chem.* **287**, 32254–32262 (2012).
11. Li, J. et al. Indole *N*-linked hydroperoxyl adduct of protein-derived cofactor modulating catalase-peroxidase functions. *Angew. Chem. Int Ed.* **63**, e202407018 (2024).
12. Yamada, Y., Fujiwara, T., Sato, T., Igarashi, N. & Tanaka, N. The 2.0 Å crystal structure of catalase-peroxidase from *Haloarcula marismortui*. *Nat. Struct. Biol.* **9**, 691–695 (2002).
13. Carpena, X. et al. Catalase-peroxidase KatG of *Burkholderia pseudomallei* at 1.7 Å resolution. *J. Mol. Biol.* **327**, 475–489 (2003).
14. Bertrand, T. et al. Crystal structure of *Mycobacterium tuberculosis* catalase-peroxidase. *J. Biol. Chem.* **279**, 38991–38999 (2004).
15. Kamachi, S., Wada, K., Tamoi, M., Shigeoka, S. & Tada, T. The 2.2.Å resolution structure of the catalase-peroxidase KatG from *Synechococcus elongatus* PCC7942. *Acta Crystallogr Sect. F. Struct. Biol. Cryst. Commun.* **70**, 288–293 (2014).
16. Liu, A. Catalase-peroxidase (KatG): a potential frontier in tuberculosis drug development. *Crit. Rev. Biochem Mol. Biol.* **59**, 434–446 (2024).
17. Njuma, O. J., Ndontsa, E. N. & Goodwin, D. C. Catalase in peroxidase clothing: Interdependent cooperation of two cofactors in the catalytic versatility of KatG. *Arch. Biochem. Biophysics* **544**, 27–39 (2014).
18. Noren, C. J., Anthony-Cahill, S. J., Griffith, M. C. & Schultz, P. G. A general method for site-specific incorporation of unnatural amino acids into proteins. *Science* **244**, 182–188 (1989).
19. Li, J. et al. Cleavage of a carbon–fluorine bond by an engineered cysteine dioxygenase. *Nat. Chem. Biol.* **14**, 853–860 (2018).
20. Wang, Y. et al. Cofactor biogenesis in cysteamine dioxygenase: C–F bond cleavage with genetically incorporated unnatural tyrosine. *Angew. Chem. Int Ed.* **57**, 8149–8153 (2018).
21. Li, J., Davis, I., Griffith, W. P. & Liu, A. Formation of monofluorinated radical cofactor in galactose oxidase through copper-mediated C–F bond scission. *J. Am. Chem. Soc.* **142**, 18753–18757 (2020).
22. Li, J., Koto, T., Davis, I. & Liu, A. Probing the Cys-Tyr cofactor biogenesis in cysteine dioxygenase by the genetic incorporation of fluorotyrosine. *Biochemistry* **58**, 2218–2227 (2019).
23. Englert, M. et al. Probing the active site tryptophan of *Staphylococcus aureus* thioredoxin with an analog. *Nucleic Acids Res* **43**, 11061–11067 (2015).
24. Ortmayer, M. et al. A noncanonical tryptophan analogue reveals an active site hydrogen bond controlling ferryl reactivity in a heme peroxidase. *JACS Au* **1**, 913–918 (2021).
25. Varnado, C. L. & Goodwin, D. C. System for the expression of recombinant hemoproteins in Escherichia coli. *Protein Expr. Purif.* **35**, 76–83 (2004).
26. Shi, X. et al. Hydroxytryptophan biosynthesis by a family of heme-dependent enzymes in bacteria. *Nat. Chem. Biol.* **19**, 1415–1422 (2023).
27. Kappock, T. J. & Caradonna, J. P. Pterin-dependent amino acid hydroxylases. *Chem. Rev.* **96**, 2659–2756 (1996).
28. Mansuy, D. et al. Thiophene S-oxides as new reactive metabolites: formation by cytochrome P-450 dependent oxidation and reaction with nucleophiles. *J. Am. Chem. Soc.* **113**, 7825–7826 (1991).
29. Shin, I. et al. Stepwise O-atom transfer in heme-based tryptophan dioxygenase: role of substrate ammonium in epoxide ring opening. *J. Am. Chem. Soc.* **140**, 4372–4379 (2018).
30. Zhang, Y. et al. Characterization of 2-oxindole forming heme enzyme MarE, expanding the functional diversity of the tryptophan dioxygenase superfamily. *J. Am. Chem. Soc.* **139**, 11887–11894 (2017).
31. Shin, I., Wang, Y. & Liu, A. A new regime of heme-dependent aromatic oxygenase superfamily. *Proc. Natl. Acad. Sci. USA* **118**, e2106561118 (2021).
32. Ravi, J., Hills, A. E., Cerasoli, E., Rakowska, P. D. & Ryadnov, M. G. FTIR markers of methionine oxidation for early detection of oxidized protein therapeutics. *Eur. Biophys. J.* **40**, 339–345 (2011).
33. Lasch, P. et al. Hydrogen peroxide-induced structural alterations of RNase A. *J. Biol. Chem.* **276**, 9492–9502 (2001).
34. Sang, R., Noble, A. & Aggarwal, V. K. Chiral Benzothiophene Synthesis via Enantiospecific Coupling of Benzothiophene S-Oxides with Boronic Esters. *Angew. Chem. Int Ed.* **60**, 25313–25317 (2021).
35. Boyd, D. R. et al. Bacterial dioxygenase- and monooxygenase-catalysed sulfoxidation of benzo[b]thiophenes. *Org. Biomol. Chem.* **10**, 782–790 (2012).
36. Munir, A. et al. Using cryo-EM to understand antimycobacterial resistance in the catalase-peroxidase (KatG) from *Mycobacterium tuberculosis*. *Structure* **29**, 899–912.e894 (2021).
37. Su, C.-C. et al. A 'Build and Retrieve' methodology to simultaneously solve cryo-EM structures of membrane proteins. *Nat. Methods* **18**, 69–75 (2021).
38. Kruft, B. I., Magliozzo, R. S. & Jarzęcki, A. A. Density functional theory insights into the role of the methionine-tyrosine-tryptophan adduct radical in the KatG catalase reaction: O_2 release from the oxyheme intermediate. *J. Phys. Chem. A* **119**, 6850–6866 (2015).
39. Colin, J., Wiseman, B., Switala, J., Loewen, P. C. & Ivancich, A. Distinct role of specific tryptophans in facilitating electron transfer or as [Fe(IV)=O Trp$^{\bullet}$] intermediates in the peroxidase reaction of *Burkholderia pseudomallei* catalase-peroxidase: a multifrequency EPR spectroscopy investigation. *J. Am. Chem. Soc.* **131**, 8557–8563 (2009).

40. Suarez, J. et al. An oxyferrous heme/protein-based radical intermediate is catalytically competent in the catalase reaction of Mycobacterium tuberculosis catalase-peroxidase (KatG). *J. Biol. Chem.* **284**, 7017–7029 (2009).
41. Chreifi, G. et al. Crystal structure of the pristine peroxidase ferryl center and its relevance to proton-coupled electron transfer. *Proc. Natl. Acad. Sci. USA* **113**, 1226–1231 (2016).
42. Casadei, C. M. et al. Heme enzymes. Neutron cryo-crystallography captures the protonation state of ferryl heme in a peroxidase. *Science* **345**, 193–197 (2014).
43. Huyett, J. E. et al. Compound ES of cytochrome c peroxidase contains a Trp pi-cation radical: Characterization by continuous wave and pulsed Q-band external nuclear double resonance spectroscopy. *J. Am. Chem. Soc.* **117**, 9033–9041 (1995).
44. Jiang, H. K. et al. Probing the active site of deubiquitinase USP30 with noncanonical tryptophan analogues. *Biochemistry* **59**, 2205–2209 (2020).
45. Pipirou, Z. et al. Peroxide-dependent formation of a covalent link between Trp51 and the heme in cytochrome c peroxidase. *Biochemistry* **48**, 3593–3599 (2009).
46. Pipirou, Z. et al. The reactivity of heme in biological systems: autocatalytic formation of both tyrosine-heme and tryptophan-heme covalent links in a single protein architecture. *Biochemistry* **46**, 13269–13278 (2007).
47. Pipirou, Z. et al. Autocatalytic formation of a covalent link between tryptophan 41 and the heme in ascorbate peroxidase. *Biochemistry* **46**, 2174–2180 (2007).
48. Dunford, H. B. Peroxidase-catalyzed halide ion oxidation. *Redox Rep.* **5**, 169–171 (2000).
49. Ortiz de Montellano, P. R. Catalytic sites of hemoprotein peroxidases. *Annu Rev. Pharm. Toxicol.* **32**, 89–107 (1992).
50. Colonna, S. et al. Enantioselective oxidations of sulfides catalyzed by chloroperoxidase. *Biochemistry* **29**, 10465–10468 (1990).
51. Casella, L. et al. Mechanism of enantioselective oxygenation of sulfides catalyzed by chloroperoxidase and horseradish peroxidase. Spectral studies and characterization of enzyme-substrate complexes. *Biochemistry* **31**, 9451–9459 (1992).
52. Ten Brink, H. B. et al. Enantioselective sulfoxidation catalyzed by vanadium haloperoxidases. *Inorg. Chem.* **37**, 6780–6784 (1998).
53. Colonna, S., Gaggero, N. & Pasta, P. Enantioselective Sulfoxidations Catalyzed by Chloroperoxidase and Horseradish Peroxidase. In: *Microbial Reagents in Organic Synthesis* (ed Servi S.). Springer Netherlands (1992).
54. Linde, D. et al. Asymmetric sulfoxidation by engineering the heme pocket of a dye-decolorizing peroxidase. *Catal. Sci. Technol.* **6**, 6277–6285 (2016).
55. Lubis, A. B. et al. Monooxygenase activity of indoleamine 2,3-dioxygenase. *J. Am. Chem. Soc.* **148**, 6178–6187 (2026).
56. Dornevil, K. et al. Cross-linking of dicyclotyrosine by the cytochrome P450 enzyme CYP121 from *Mycobacterium tuberculosis* proceeds through a catalytic shunt pathway. *J. Biol. Chem.* **292**, 13645–13657 (2017).
57. Fielding, A. J., Dornevil, K., Ma, L., Davis, I. & Liu, A. Probing ligand exchange in the P450 Enzyme CYP121 from *Mycobacterium tuberculosis*: dynamic equilibrium of the distal heme ligand as a function of pH and temperature. *J. Am. Chem. Soc.* **139**, 17484–17499 (2017).
58. Duan, R., Li, J., Nathan, B., Yang, X. & Liu, A. CryoEM structure of EcKatG S-Trp105 at 2.22 Å resolution revealing an asymmetric sulfur center in O=S-Trp. *RCSB PDB*, https://doi.org/10.2210/pdb9O6A/pdb (2025).

Acknowledgements

We thank Dr. Douglas C. Goodwin for providing the initial KatG expression system for our optimization and Dr. Audrey Lamb and Dr. Ruyan Guo for providing access to their CD and IR spectrophotometers, respectively. We are grateful to Dr. Iram Aziz for her help with the cryo-EM image analysis on an initial lower-resolution dataset.

Author contributions

R.D. and J.L. optimized the KatG expression system and carried out the genetic incorporation of S-Trp. A.P.G. provided the pEVOL_PylRS_S-Trp plasmid. R.D. performed protein expression, purification, enzyme assays, and biophysical spectroscopic analyses. R.D. and W.P.G. conducted protein digestion and mass spectrometry. R.D. prepared samples for cryo-EM; Y.X. and N.D.B. prepared cryo-EM grids, and Y.X. collected the cryo-EM data. R.D. and J.L., with guidance from Y.X. and N.D.B., analyzed and interpreted the cryo-EM data. R.D., J.L., and A.L. drafted the initial manuscript. A.L. conceived and supervised the project. All authors contributed to data analysis and to writing and revising the manuscript.

Funding

This research was primarily supported by the National Institutes of Health (NIH) grant GM152982. The National Science Foundation Grant CHE-2204225, Welch Foundation award AX-2110-20250403, and Lutcher Brown Distinguished Chair in Biochemistry Endowment for concept development provided additional support. The Mass Spectrometry data was collected at the UTSA Mass Spectrometry & Proteomics Facility. The cryo-EM data collection was supported by the S^2C^2 User Program at the Stanford-SLAC CryoEM Center under the user project CE80, with the program supported by the NIH Common Fund transformative high-resolution cryoEM program (U24 GM129541).

Competing interests

The authors declare no competing interests.

Additional information

Supplementary information The online version contains supplementary material available at https://doi.org/10.1038/s41467-026-73579-y.

Correspondence and requests for materials should be addressed to Aimin Liu.

Peer review information *Nature Communications* thanks Stephen Carr and the other, anonymous, reviewers for their contribution to the peer review of this work. A peer review file is available.

Supplementary Information

Single-atom substitution redirects KatG reactivity from cofactor biogenesis to stereoselective sulfoxidation

Ran Duan,[1] Jiasong Li,[1,Δ] Wendell P. Griffith,[1] Yang Xu,[2] Nathan D. Burrows,[2] Anthony P. Green,[3] and Aimin Liu[*,†,1]

[1] Department of Chemistry, The University of Texas at San Antonio, San Antonio, TX 78249, USA
[2] Division of CryoEM and Bioimaging, Stanford Synchrotron Radiation Lightsource, SLAC National Accelerator Laboratory, Stanford University, Menlo Park, CA 94025, USA
[3] Manchester Institute of Biotechnology and Department of Chemistry, The University of Manchester, Manchester, M1 7DN, UK

[Δ] Current Address: Key Laboratory of Agricultural Environmental Microbiology, Ministry of Agriculture, College of Life Sciences, Nanjing Agricultural University, Nanjing, 210095, P. R. China

[†] Current Address: Department of Biochemistry and Biophysics, and Department of Chemistry, University of Pennsylvania, Philadelphia, PA 19104, USA

* Correspondence Author: Prof. Dr. Aimin Liu, E-mail: Feradical@utsa.edu

Table of Content

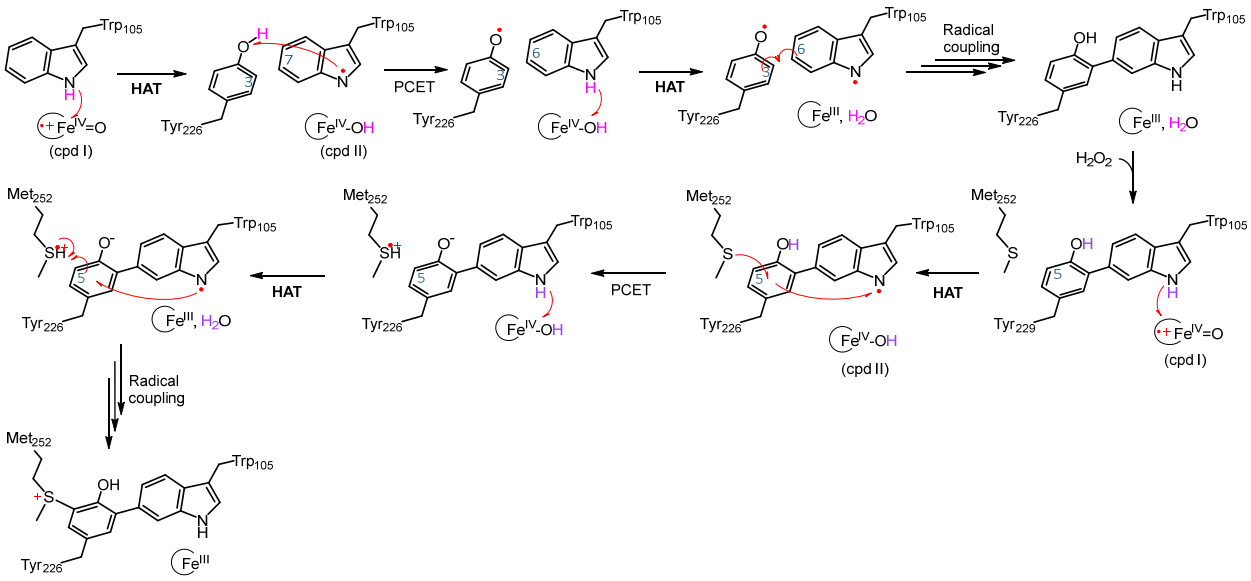

Supplementary figure 1. A proposed mechanism for MYW biogenesis involves four hydrogen atom transfer (HAT) steps on the indole N–H moiety in two rounds of heme-mediated H_2O_2 oxidation.

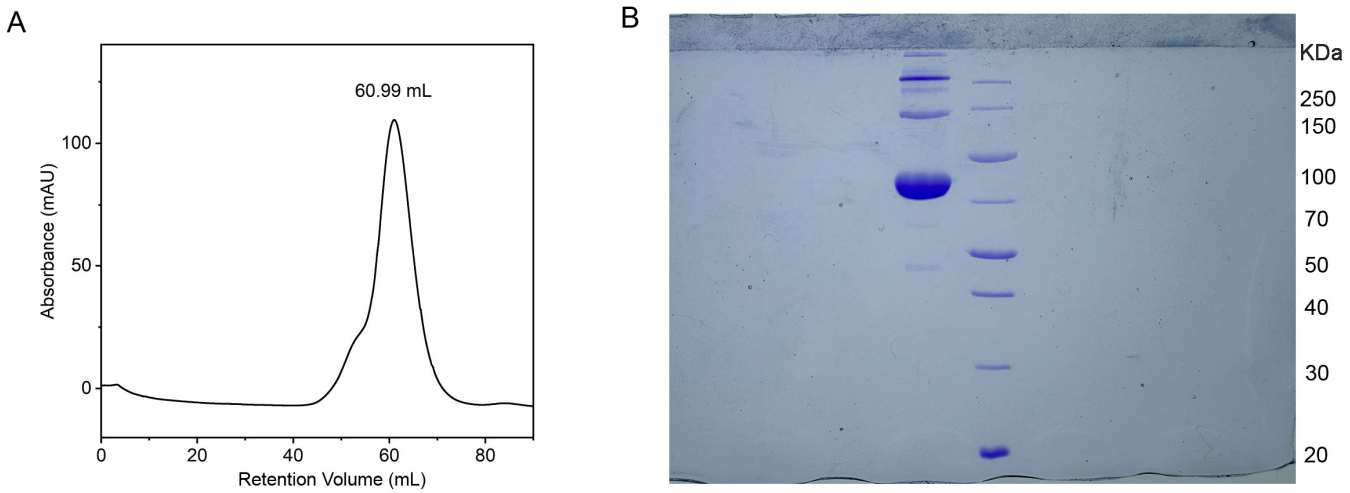

Supplementary figure 2. Purification of EcKatG S-Trp105. (A) Gel-filtration chromatography of as-isolated KatG S-Trp105 using a HiLoad 16/600 Superdex 200 column in 50 mM NaPi buffer (pH 7.0) at a 1.5 mL/min. (B) SDS-PAGE analysis of purified KatG S-Trp105 protein. The molecular weight markers are indicated on the right.

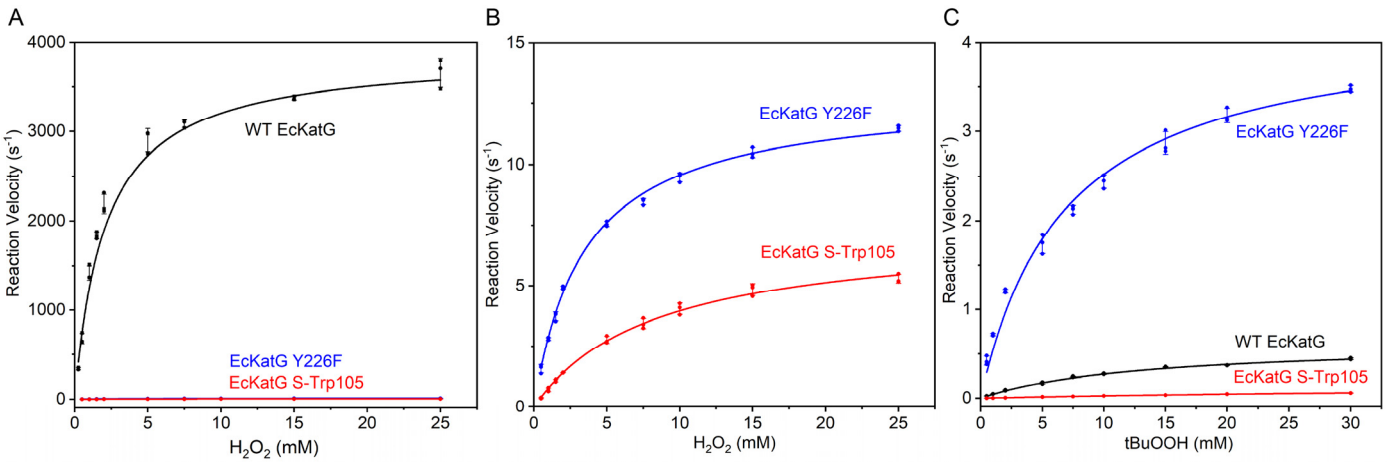

Supplementary figure 3. Catalase and peroxidase activities of WT, S-Trp105, and Y226F EcKatG proteins. (A) Catalase activity comparison. (B) Magnified view of catalase activities for KatG S-Trp105 and KatG Y226F. (C) Peroxidase activity comparison. Activities for WT (black), KatG S-Trp105 (red), and KatG Y226F (blue) are shown. Individual data points are overlaid on each bar. Error bars represent mean ± SD (n = 3 independent technical replicates).

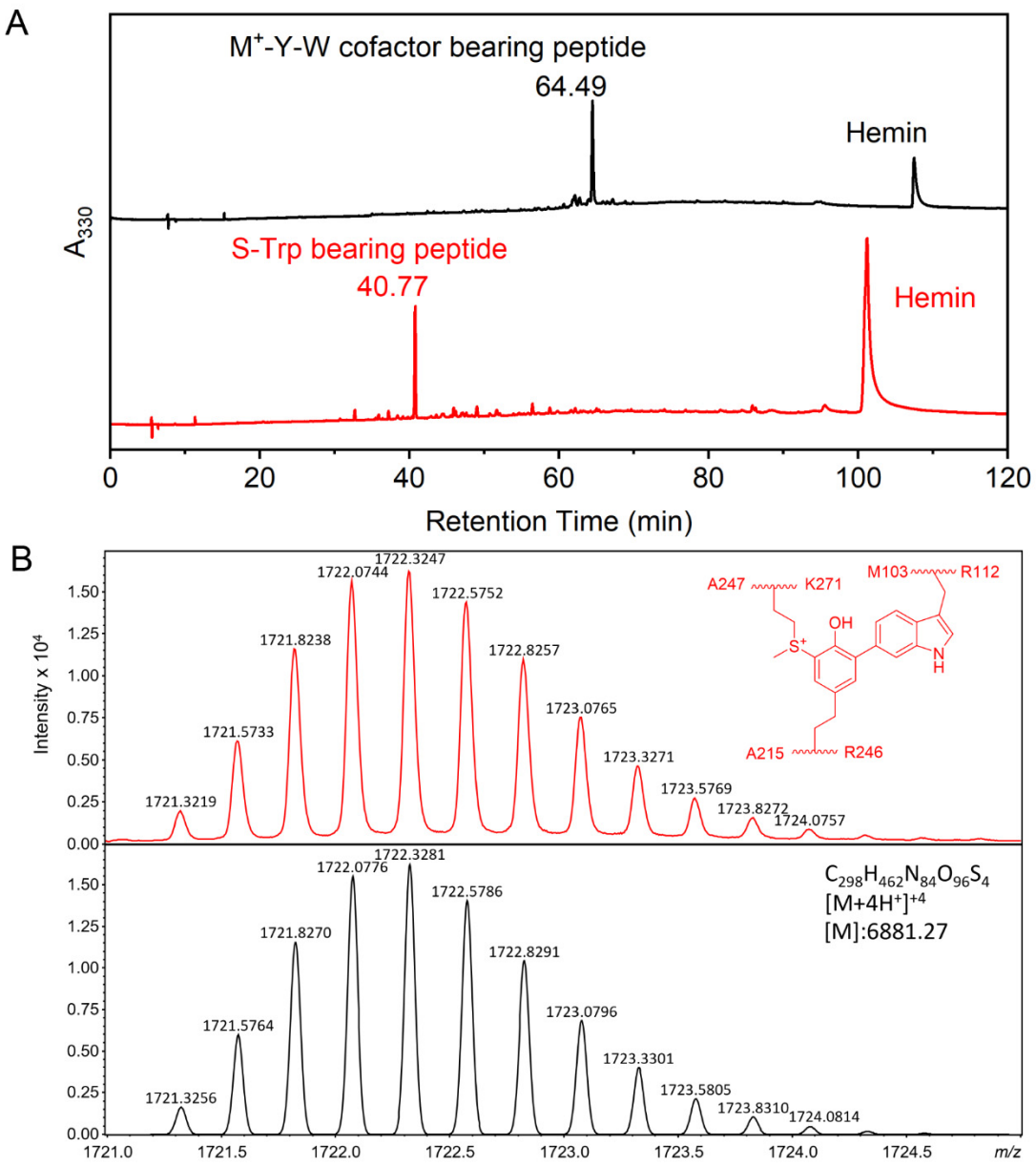

Supplementary figure 4. HPLC and HRMS analysis of the MYW cofactor-bearing peptide in WT KatG. (A) Comparison of HPLC profiles for the MYW cofactor peptide in WT KatG (black) and the corresponding S-Trp-bearing peptide in KatG S-Trp105 (red), highlighting their distinct retention times. (B) High-resolution mass spectrum (HRMS) of the MYW cofactor-bearing peptide from WT EcKatG (red) overlaid with the simulated spectrum (black).

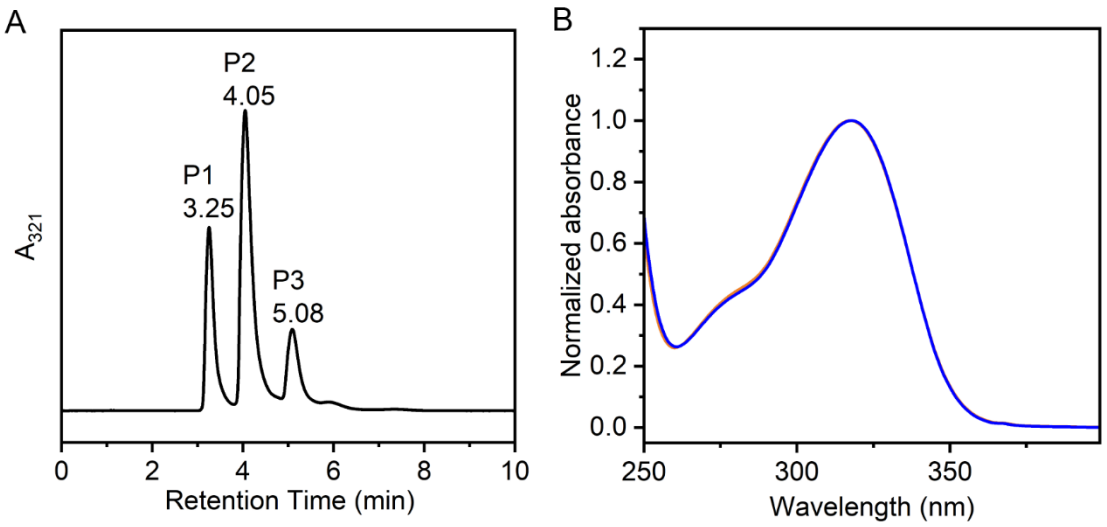

Supplementary figure 5. HPLC separation and UV-vis spectra of S-monooxygenated S-Trp diastereomers. (A) Preparative HPLC chromatogram showing the separation of S-monooxygenated S-Trp products (P1 and P2). (B) Comparison of UV-vis spectra for fractions P1 (orange) and P2 (blue).

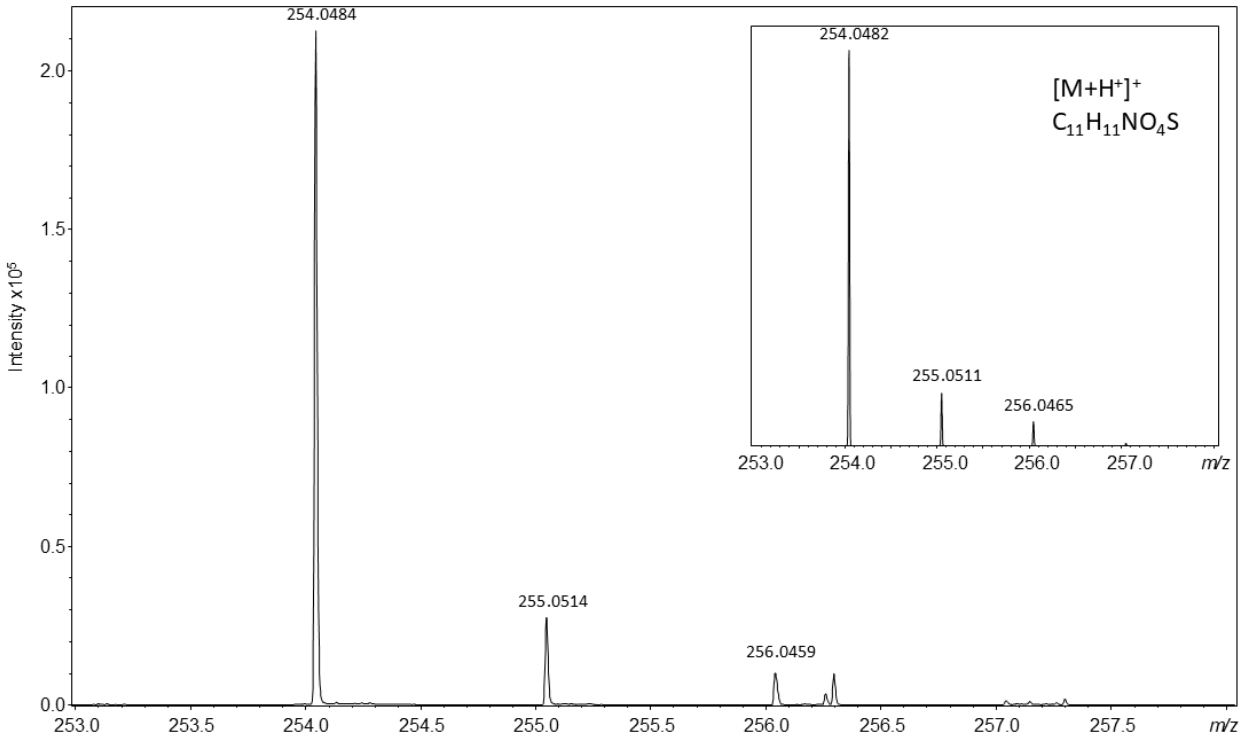

Supplementary figure 6. High-resolution mass spectrum of fraction P3 in Supplementary figure 5 showing experimental and simulated (inset) isotope distributions for 2-amino-3-(1,1-dioxidobenzo[b]thiophen-3-yl)propanoic acid ($C_{11}H_{11}NO_4S$).

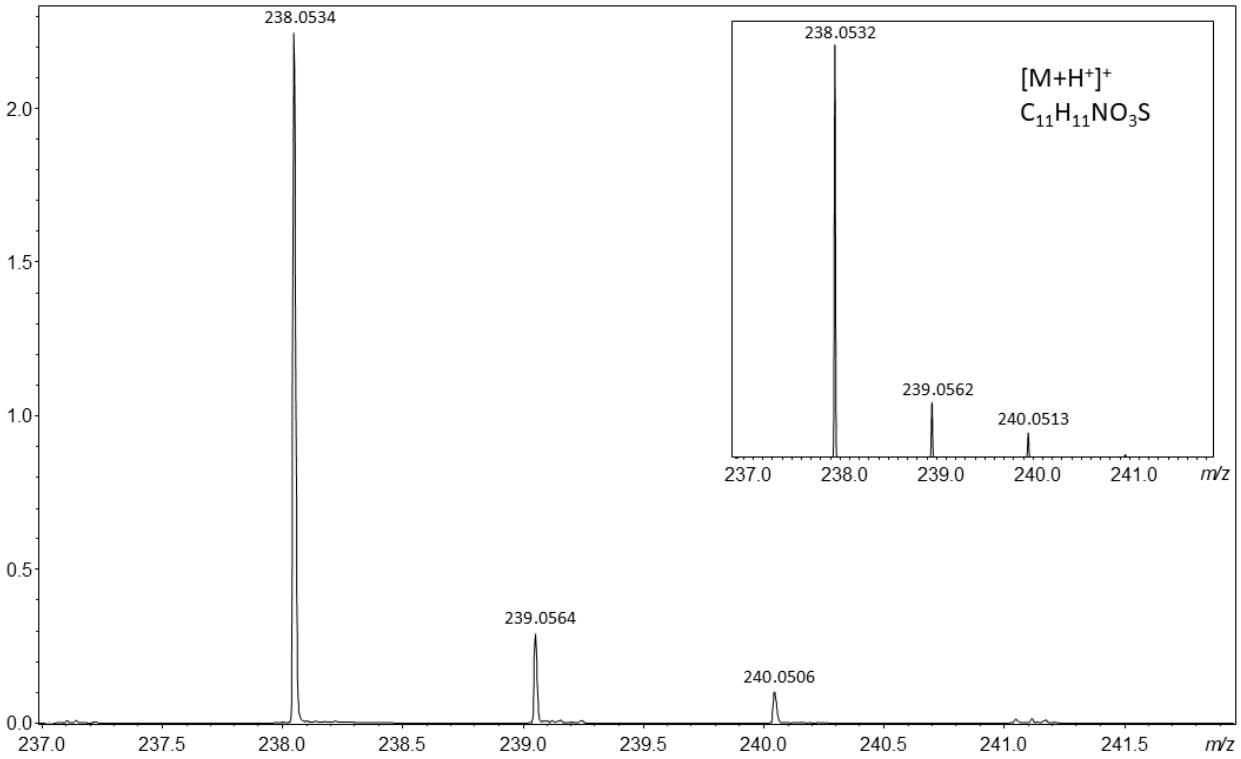

Supplementary figure 7. High-resolution mass spectrum of fraction P1 in Supplementary figure 5 showing experimental and simulated (inset) isotope distributions for 2-amino-3-(1-oxidobenzo[b]thiophen-3-yl)propanoic acid ($C_{11}H_{11}NO_3S$).

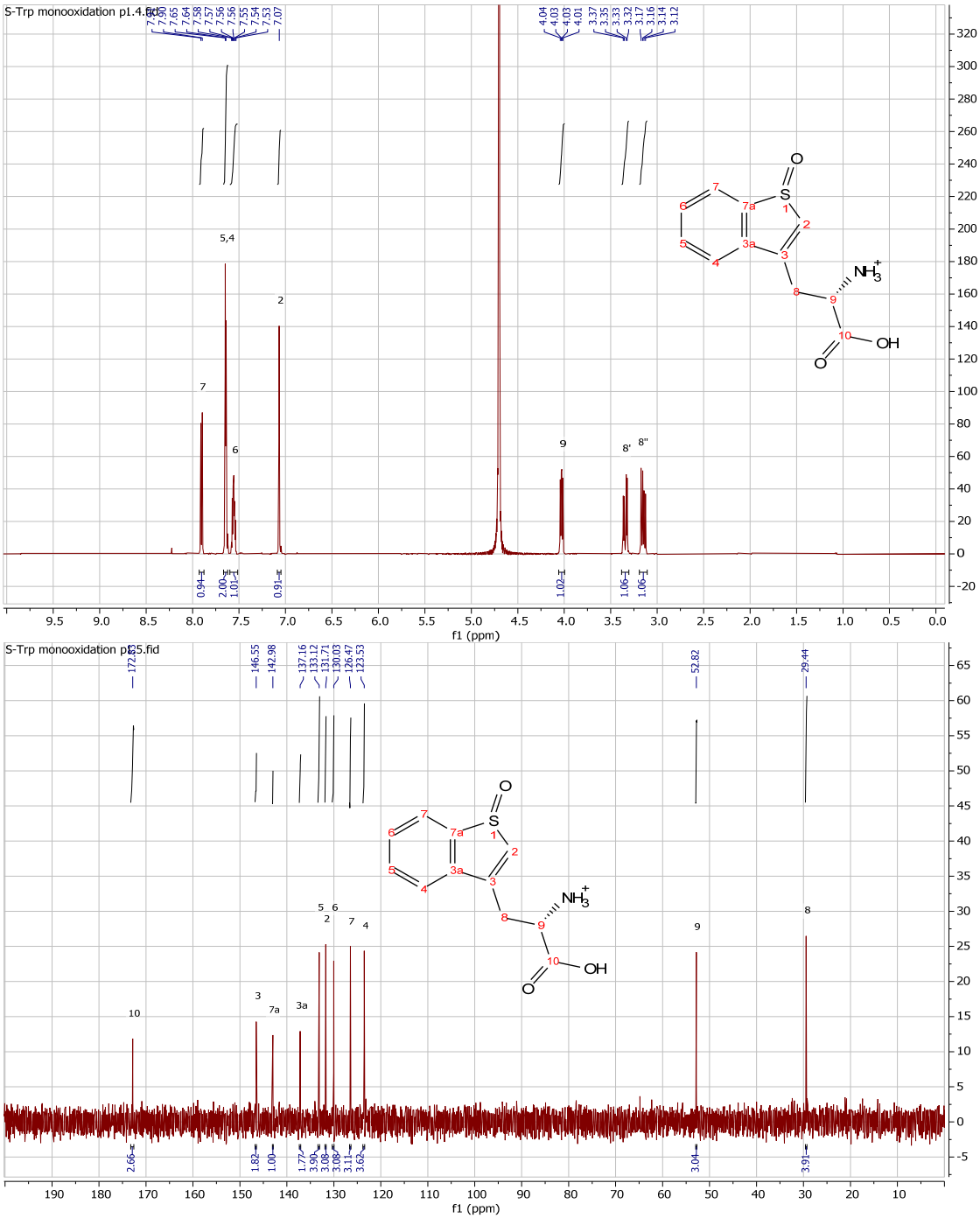

Supplementary figure 8. ^{1}H NMR (500 MHz, D_2O) and ^{13}C NMR (126 MHz, D_2O) spectra of fraction P1 in Supplementary figure 5.

^{1}H NMR (500 MHz, D_2O) δ 7.90 (d, J = 7.7 Hz, ^{1}H), 7.64 (d, J = 4.0 Hz, ^{2}H), 7.56 (dq, J = 8.3, 4.3 Hz, ^{1}H), 7.07 (s, ^{1}H), 4.03 (dd, J = 8.6, 5.4 Hz, ^{1}H), 3.34 (dd, J = 15.6, 5.4 Hz, ^{1}H), 3.15 (dd, J = 15.6, 8.6 Hz, ^{1}H). ^{13}C NMR (126 MHz, D_2O) δ 172.83, 146.55, 142.98, 137.16, 133.12, 131.71, 130.03, 126.47, 123.53, 52.82, 29.44.

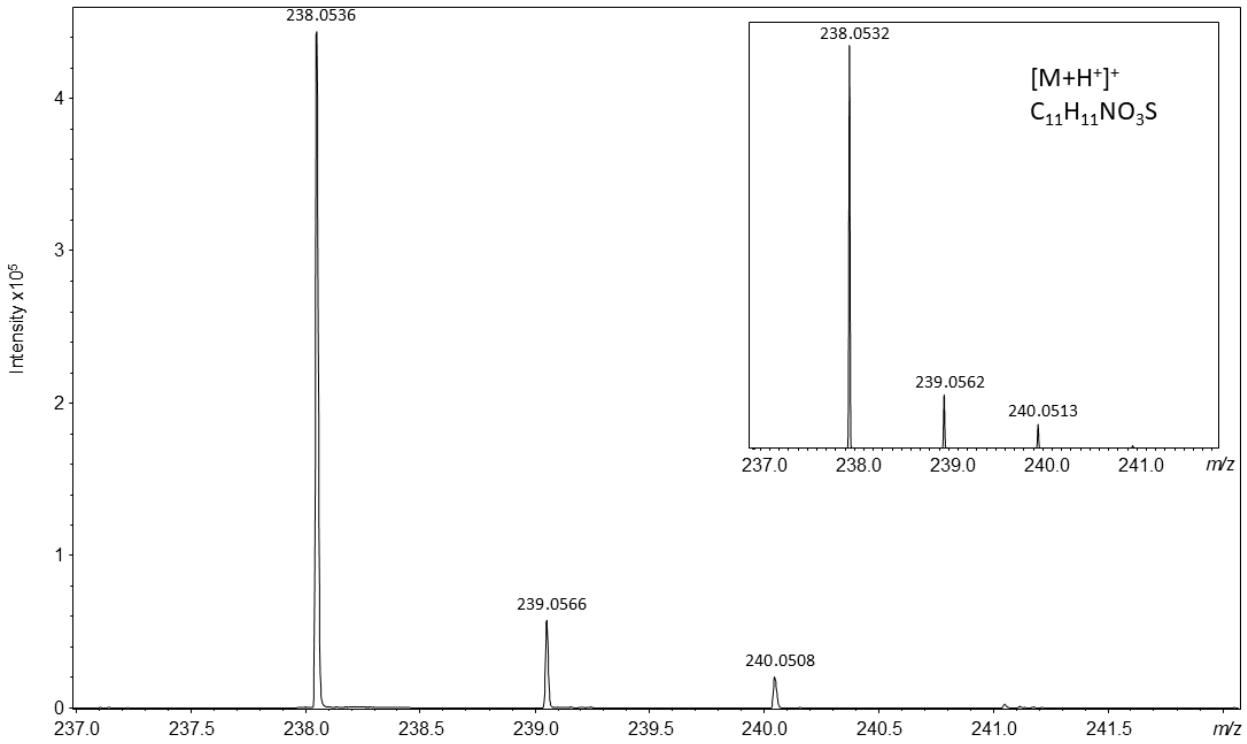

Supplementary figure 9. High-resolution mass spectrum of fraction P2 in Supplementary figure 5 showing experimental and simulated (inset) isotope distributions for 2-amino-3-(1-oxidobenzo[b]thiophen-3-yl)propanoic acid ($C_{11}H_{11}NO_3S$).

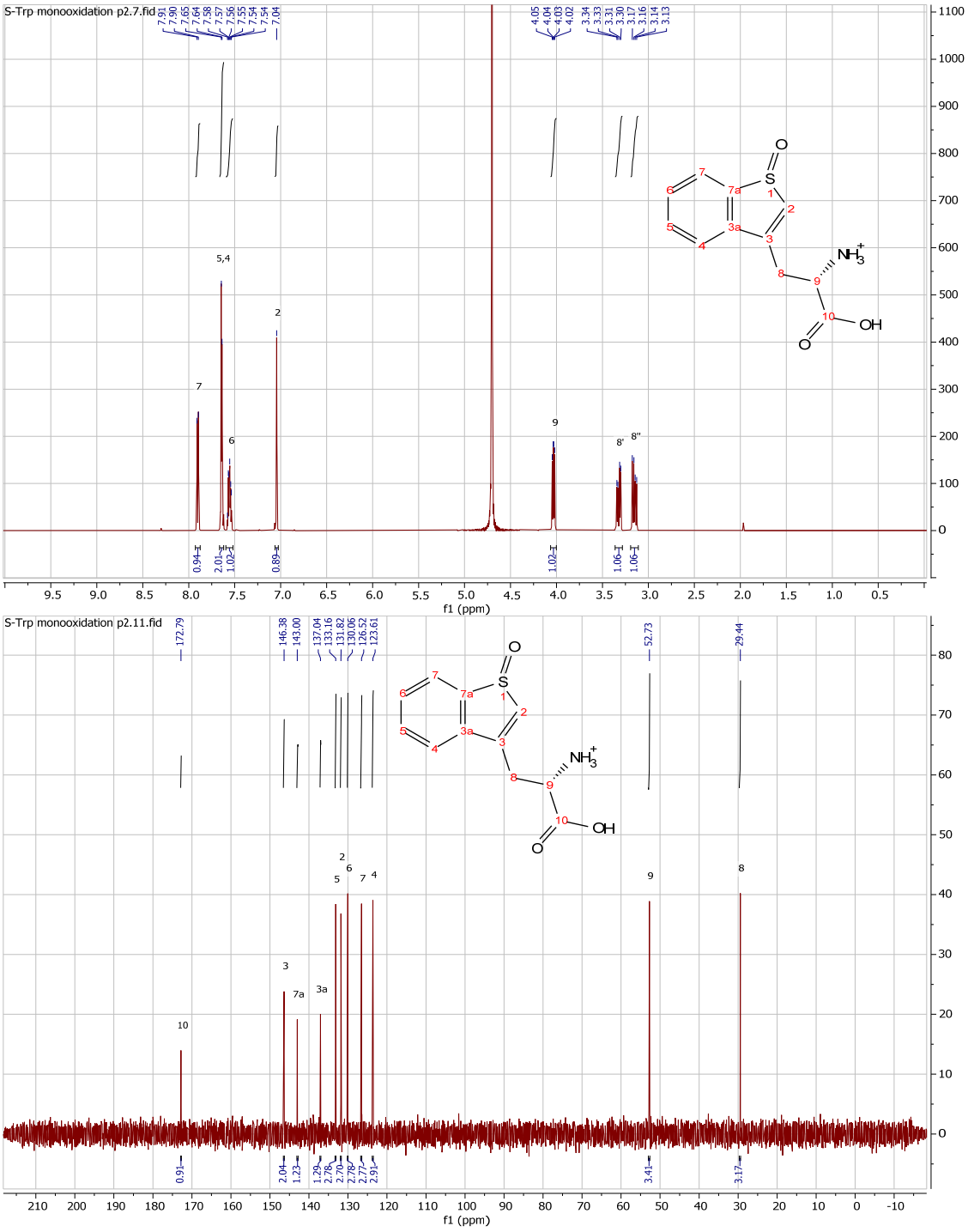

Supplementary figure 10. ^{1}H NMR (500 MHz, D_2O) and ^{13}C NMR (126 MHz, D_2O) spectra of fraction P2 in Supplementary figure 5.

^{1}H NMR (500 MHz, D_2O) δ 7.90 (dd, J = 7.5, 0.9 Hz, ^{1}H), 7.64 (d, J = 4.2 Hz, ^{2}H), 7.55 (dq, J = 8.3, 3.5 Hz, ^{1}H), 7.04 (s, ^{1}H), 4.03 (dd, J = 8.2, 5.6 Hz, ^{1}H), 3.32 (dd, J = 15.4, 5.6 Hz, ^{1}H), 3.15 (dd, J = 15.4, 8.2 Hz, ^{1}H).
^{13}C NMR (126 MHz, D_2O) δ 172.79, 146.38, 143.00, 137.04, 133.16, 131.82, 130.06, 126.52, 123.61, 52.73, 29.44.

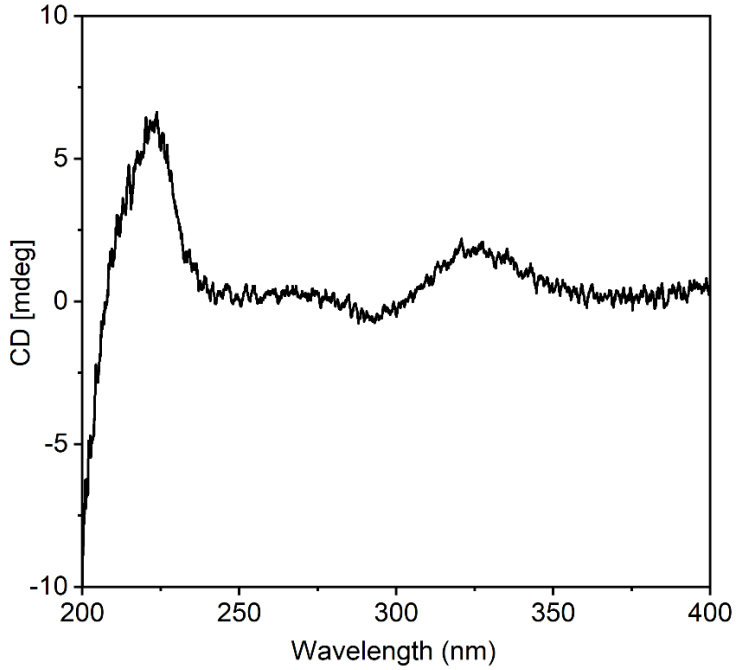

Supplementary figure 11. Original circular dichroism (CD) spectrum of the S-Trp105-bearing peptide isolated from digested KatG S-Trp105 via HPLC.

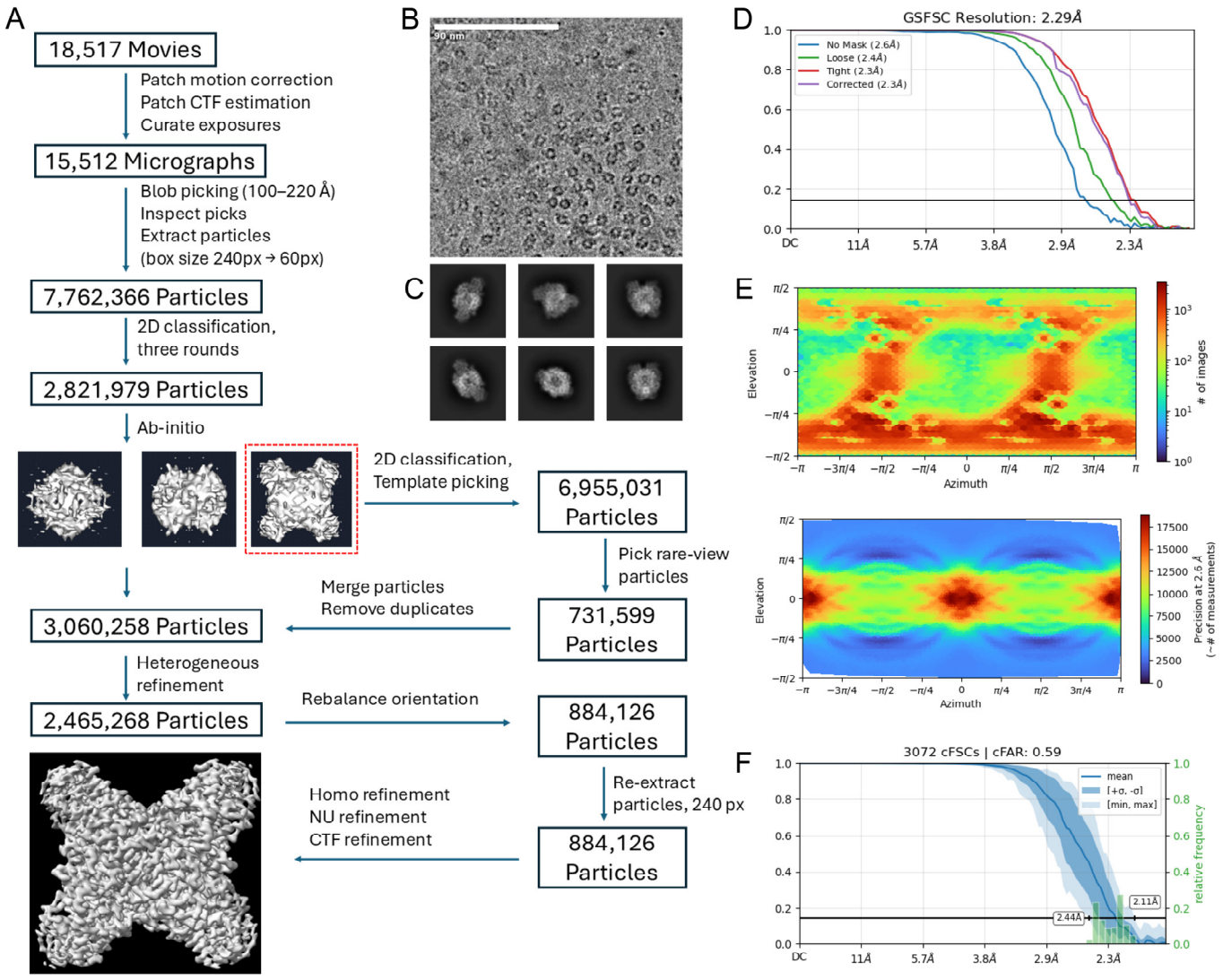

Supplementary figure 12. Cryo-EM data processing workflow. (A) A flow chart illustrates the cryo-EM data processing pipeline, (B) Representative cryo-EM micrograph, (C) Representative 2D class averages, (D) Gold-standard Fourier shell correlation (GSFSC) curves of the final reconstruction, (E) Viewing direction distribution and posterior precision directional distribution of particles used in the final reconstruction, and (F) Directional FSC plot of the final reconstruction.

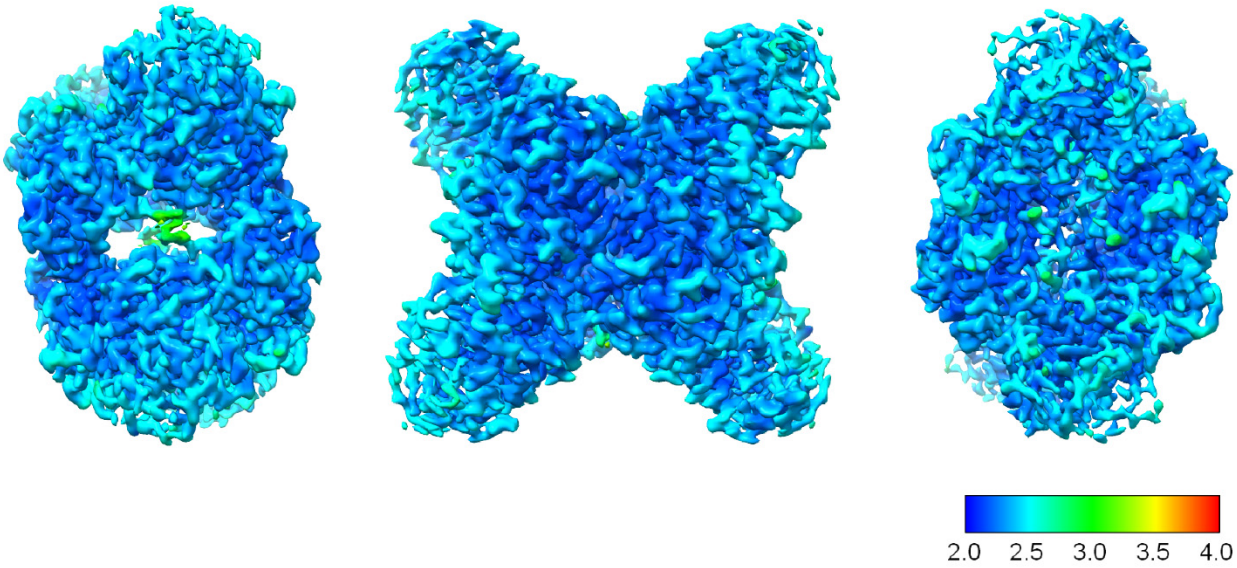

Supplementary figure 13. Local resolution of the cryo-EM density map. Local resolution map of the raw cryo-EM density map calculated using CryoSPARC and visualized with ChimeraX. Side, front, and top views are shown, with the resolution scale (in Å) at the bottom right.

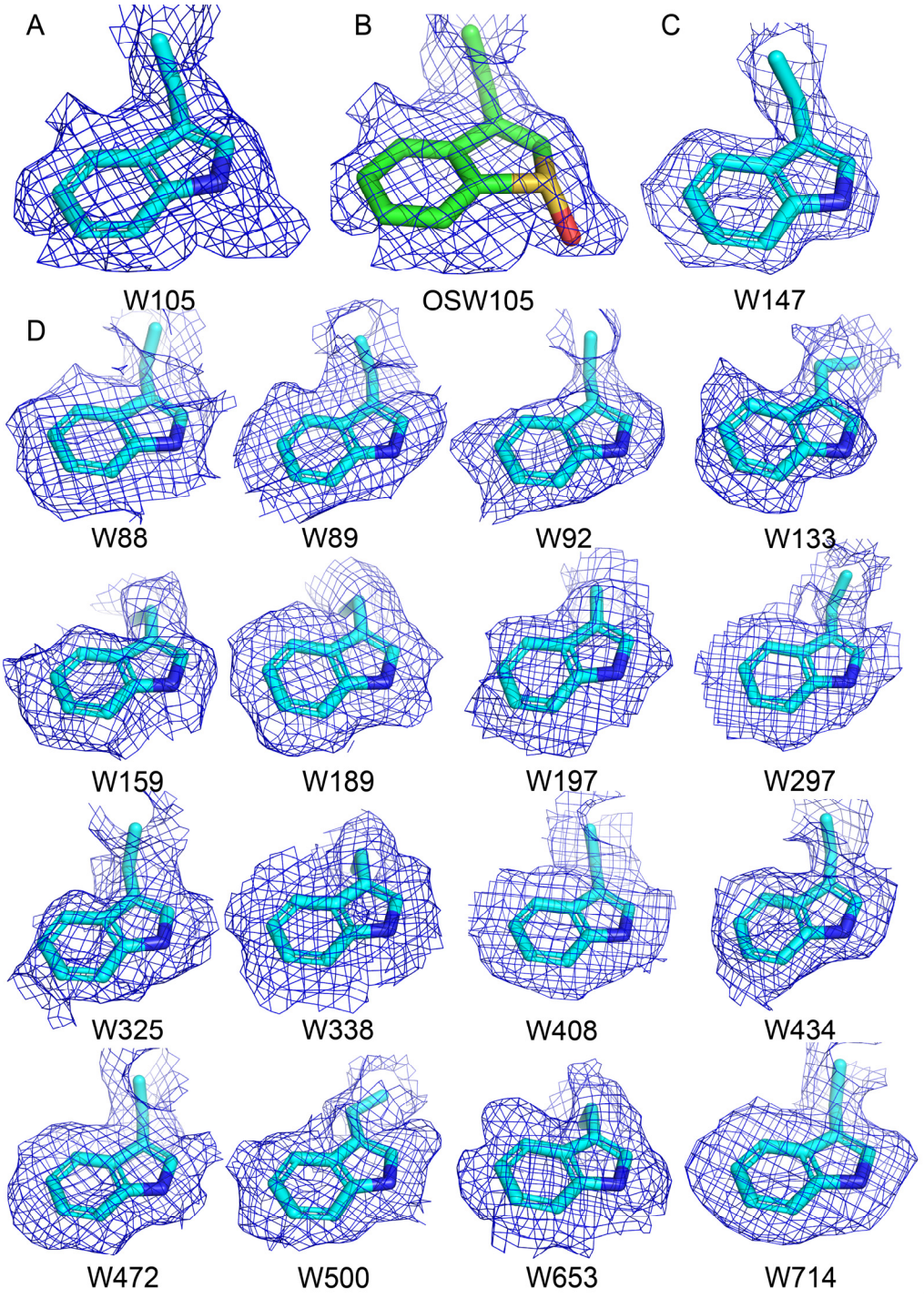

Supplementary figure 14. Comparison of density map and model fitting on monooxygenated S-Trp (molecular code in the structure: OSW) vs. unmodified Trp residues: (A) OSW105 density map fit with L-Trp; (B) OSW (W*) density map fit with OSW; (C) Density map and model for W147; (D) Density map and model for all other Trp residues in the chain A of KatG S-Trp105 protein

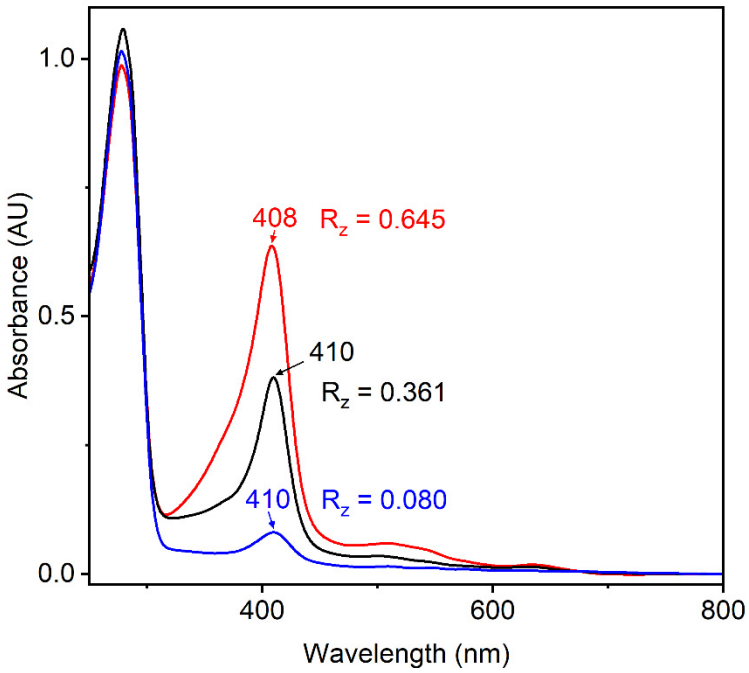

Supplementary figure 15. UV-vis and R_z value comparison of KatG S-Trp105, apo-KatG S-Trp105, and heme-reconstituted KatG S-Trp105. UV-vis spectra and corresponding R_z values are shown for as-isolated KatG S-Trp105 (black), apo-KatG S-Trp105 (blue), and heme-reconstituted KatG S-Trp105 (red).

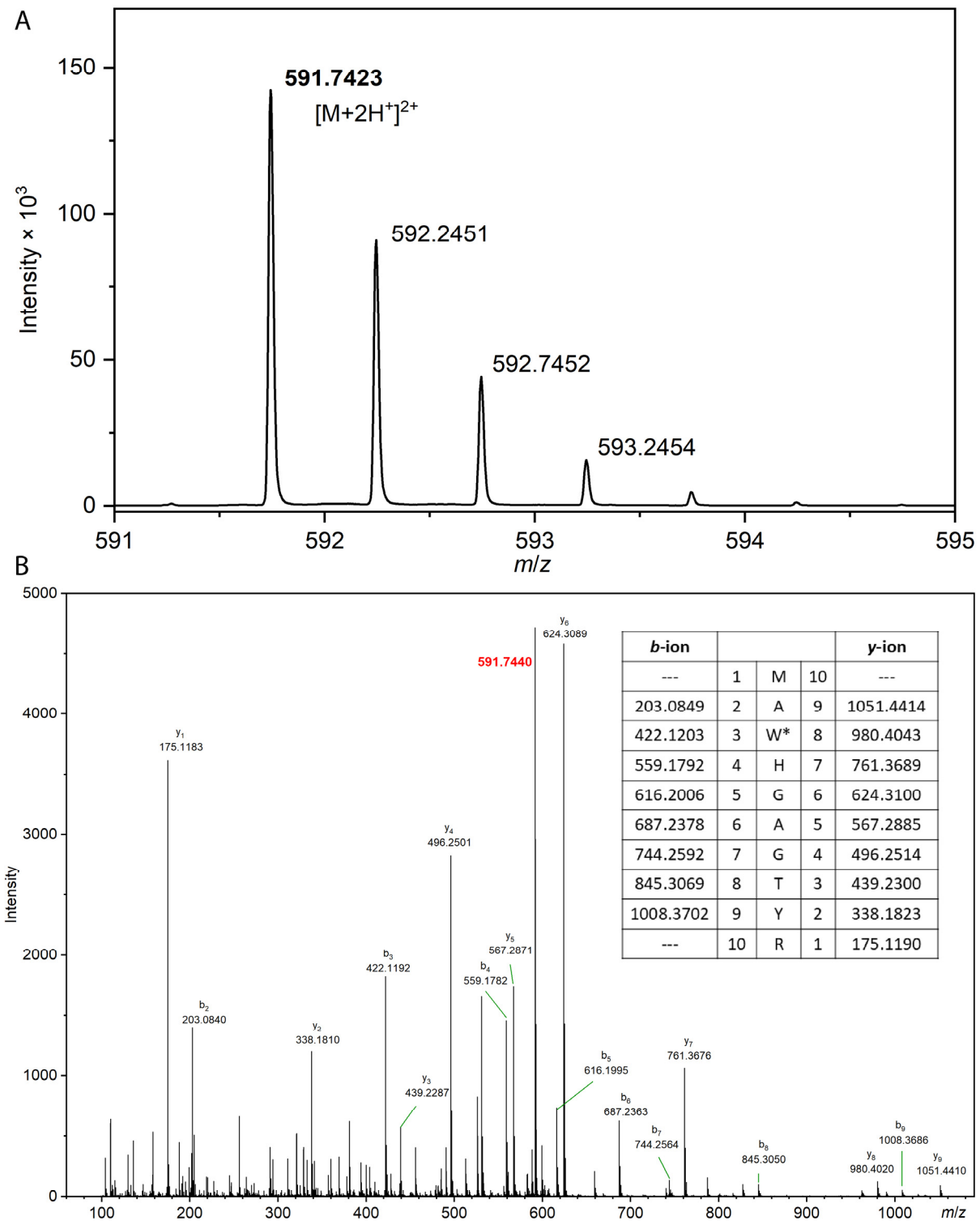

b-ion				*y*-ion
---	1	M	10	---
203.0849	2	A	9	1051.4414
422.1203	3	W*	8	980.4043
559.1792	4	H	7	761.3689
616.2006	5	G	6	624.3100
687.2378	6	A	5	567.2885
744.2592	7	G	4	496.2514
845.3069	8	T	3	439.2300
1008.3702	9	Y	2	338.1823
---	10	R	1	175.1190

Supplementary figure 16. HRMS spectrum (A) and CID spectrum (B) for regenerated O=S-Trp bearing peptide. The inset shows the fragment ion assignments.

Supplementary table 1. Fragment assignment for the CID spectrum in Figure 3C

Residue formula for W*	$C_{11}H_9N_1O_2S_1$					
Predicted b-ions	Detected b-ions	b-ion	Residues	y-ion	Detected y-ions	Predicted y-ions
---		1	M	10		---
203.0849	203.0851	2	A	9	1051.4436	1051.4414
422.1203	422.1208	3	W*	8	980.4028	980.4043
559.1792	559.1800	4	H	7	761.3696	761.3689
616.2006	616.2013	5	G	6	624.3105	624.3100
687.2378	687.2385	6	A	5	567.2893	567.2885
744.2592	744.2599	7	G	4	496.2521	496.2514
845.3069	845.3064	8	T	3	439.2300	439.2300
1008.3702	1008.3702	9	Y	2	338.1826	338.1823
---		10	R	1	175.1190	175.119

The monooxygenated S-Trp residue was assigned as W*.
Theoretical masses for the b- and y-type fragment ions were calculated using the MS-Product utility of ProteinProspector (https://prospector.ucsf.edu/prospector/mshome.htm) using [$C_{11}H_9NO_2S$] for the monooxygenated S-Trp residue (W*).

Supplementary table 2. Cryo-EM data collection, processing, and refinement statistics
(PDB DOI: https://doi.org/10.2210/pdb9O6A/pdb; EMDB: https://www.ebi.ac.uk/emdb/EMD-70168)

	S-Trp105 EcKatG
Deposited Files	EMDB-70168; PDB-9O6A
Data Collection and Processing	SSRL
Electron Microscope	Titan Krios G3i
Voltage (kV)	300 keV
Camera	Falcon 4i
Defocus range (μm)	-1.0 ~ -2.0
Total exposure time (s)	6.58
Energy filter width (eV)	10
Pixel size (Å) (calibrated)	0.954
Total dose (e-/Å2)	50
Number of frames	38
Does per frame ($e^-/Å^2$)	1.1357
Magnification (nominal)	130,000×
No. of initial micrographs	15512
No. of initial particles	7,762,366
No. of final particles	884,126
Symmetry	D2
Map Resolution (Å)	2.29
FSC threshold	0.143
Density modification Resolution (Å)	2.22
Refinement and Validation	
Map-sharping B-factors (Å2)	-7.92
Model composition	
Chain	4
Protein residues	2576
Ligands (heme)	4
r.m.s. deviationsa	
Bond lengthsd (Å)	0.003
Bond angles (°)	0.601592
MolProbity score	1.0819
Ramachandrane	
Favored (%)	98.4778
Allowed (%)	1.4918
Outlier (%)	0.04
ADP (B-factors) (min/max/mean) ($Å^2$)	
Protein	0.01/77.15/20.17
Ligand	8.43/29.45/16.19
CCb Mask	0.79

[a]root means square deviation
[b]correlation coefficient

Supplementary table 3. The stereochemical restraints of O=S-Trp during cryo-EM data processing. The restraints were established based on reported small-molecule structures of benzothiophene S-oxide analogs listed in the table.

3D structure	Bond length (Å)	Bond angle (°)	CCDC number	Reference
	S-C1	C1-S-C2		
	S-C2	C1-S-O		
	S-O	C2-S-O		
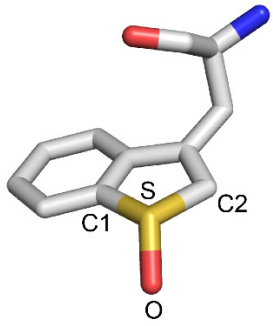	1.77 1.78 1.49	112.4 113.7 89.9	N/A	This work
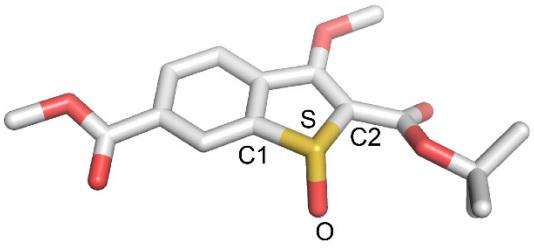	1.79 1.80 1.49	109.2 112.9 89.4	1842115	Ref. 1
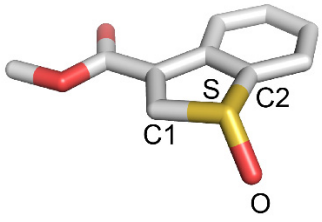	1.78 1.77 1.49	113.4 111.5 90.3	2236439	Ref. 2

The stereochemical restraints for S-monooxygenated S-Trp (OSW) are shown in a CIF file shown below.

The corresponding CIF File associated with Supplementary table 3:

```
data_comp_list
loop_
_chem_comp.id
_chem_comp.three_letter_code
_chem_comp.name
_chem_comp.group
_chem_comp.number_atoms_all
_chem_comp.number_atoms_nh
_chem_comp.desc_level
OSW        OSW 'Unknown                    ' ligand 15 15 .
#
data_comp_OSW
#
loop_
_chem_comp_atom.comp_id
_chem_comp_atom.atom_id
_chem_comp_atom.type_symbol
_chem_comp_atom.type_energy
_chem_comp_atom.charge
_chem_comp_atom.partial_charge
_chem_comp_atom.x
_chem_comp_atom.y
_chem_comp_atom.z
OSW        N     N   NH2    0    .     119.5940   84.6760  146.4100
OSW        CA    C   CH1    0    .     118.4470   84.4860  147.2410
OSW        C     C   C1     0    .     118.0770   85.7980  147.9700
OSW        O     O   O      0    .     116.9390   86.1590  148.0120
OSW        CB    C   CH2    0    .     118.6830   83.3670  148.2660
OSW        CG    C   CH1    0    .     118.0430   83.6800  149.6580
OSW        CD1   C   CH2    0    .     118.7890   83.9230  150.7400
OSW        CD2   C   CR6    0    .     116.5960   83.6100  149.9160
OSW        CE2   C   CR6    0    .     116.3310   83.8440  151.2730
OSW        CE3   C   CR16   0    .     115.5390   83.3480  149.0540
OSW        CZ2   C   CR16   0    .     115.0460   83.8240  151.7930
OSW        CZ3   C   CR16   0    .     114.2450   83.2850  149.5800
OSW        CH2   C   CR16   0    .     113.9990   83.5040  150.9370
OSW        O1    O   OH1    0    .     118.0340   83.4370  153.3300
OSW        S     S   SH1    0    .     117.7860   84.3250  152.1560
#
loop_
_chem_comp_bond.comp_id
_chem_comp_bond.atom_id_1
_chem_comp_bond.atom_id_2
_chem_comp_bond.type
```

```
_chem_comp_bond.value_dist
_chem_comp_bond.value_dist_esd
_chem_comp_bond.value_dist_neutron
OSW   N      CA    single       1.429 0.020    1.429
OSW   CA     C     single       1.546 0.020    1.546
OSW   CA     CB    single       1.536 0.020    1.536
OSW   C      O     double       1.195 0.020    1.195
OSW   CB     CG    single       1.564 0.020    1.564
OSW   CG     CD1   single       1.337 0.020    1.337
OSW   CG     CD2   single       1.471 0.020    1.471
OSW   CD1    S     single       1.781 0.020    1.781
OSW   CD2    CE2   aromatic     1.402 0.020    1.402
OSW   CD2    CE3   aromatic     1.389 0.020    1.389
OSW   CE2    CZ2   aromatic     1.386 0.020    1.386
OSW   CE2    S     single       1.769 0.020    1.769
OSW   CE3    CZ3   aromatic     1.398 0.020    1.398
OSW   CZ2    CH2   aromatic     1.390 0.020    1.390
OSW   CZ3    CH2   aromatic     1.396 0.020    1.396
OSW   O1     S     single       1.493 0.020    1.493
#
loop_
_chem_comp_angle.comp_id
_chem_comp_angle.atom_id_1
_chem_comp_angle.atom_id_2
_chem_comp_angle.atom_id_3
_chem_comp_angle.value_angle
_chem_comp_angle.value_angle_esd
OSW   CB     CA     C          109.90 3.000
OSW   CB     CA     N          111.20 3.000
OSW   C      CA     N          110.70 3.000
OSW   O      C      CA         120.07 3.000
OSW   CG     CB     CA         112.67 3.000
OSW   CD2    CG     CD1        114.56 3.000
OSW   CD2    CG     CB         123.30 3.000
OSW   CD1    CG     CB         121.91 3.000
OSW   S      CD1    CG         111.73 3.000
OSW   CE3    CD2    CE2        119.23 3.000
OSW   CE3    CD2    CG         130.43 3.000
OSW   CE2    CD2    CG         110.34 3.000
OSW   S      CE2    CZ2        125.39 3.000
OSW   S      CE2    CD2        111.90 3.000
OSW   CZ2    CE2    CD2        122.39 3.000
OSW   CZ3    CE3    CD2        118.64 3.000
OSW   CH2    CZ2    CE2        118.07 3.000
OSW   CH2    CZ3    CE3        121.44 3.000
OSW   CZ3    CH2    CZ2        120.13 3.000
```

```
OSW   O1     S      CE2        111.56 3.000
OSW   O1     S      CD1        113.42 3.000
OSW   CE2    S      CD1         90.29 3.000
#
loop_
_chem_comp_tor.comp_id
_chem_comp_tor.id
_chem_comp_tor.atom_id_1
_chem_comp_tor.atom_id_2
_chem_comp_tor.atom_id_3
_chem_comp_tor.atom_id_4
_chem_comp_tor.value_angle
_chem_comp_tor.value_angle_esd
_chem_comp_tor.period
OSW CONST_01      CH2    CZ2    CE2    CD2          2.74   0.0 0
OSW CONST_02      CH2    CZ3    CE3    CD2          1.23   0.0 0
OSW CONST_03      CZ3    CE3    CD2    CE2         -1.99   0.0 0
OSW CONST_04      CZ3    CH2    CZ2    CE2         -3.47   0.0 0
OSW CONST_05      CZ2    CE2    CD2    CE3          0.01   0.0 0
OSW CONST_06      CZ2    CH2    CZ3    CE3          1.56   0.0 0
OSW Var_01        CE2    S      CD1    CG          10.05  30.0 1
OSW Var_02        CE2    CD2    CG     CD1          1.02  30.0 1
OSW Var_03        CD2    CE2    S      CD1         -9.45  30.0 1
OSW Var_04        S      CD1    CG     CD2         -8.19  30.0 1
OSW Var_05        CD1    CG     CB     CA        -111.72  30.0 3
OSW Var_06        CG     CB     CA     N         142.24  30.0 3
OSW Var_07        O      C      CA     N         134.53  30.0 3
#
loop_
_chem_comp_chir.comp_id
_chem_comp_chir.id
_chem_comp_chir.atom_id_centre
_chem_comp_chir.atom_id_1
_chem_comp_chir.atom_id_2
_chem_comp_chir.atom_id_3
_chem_comp_chir.volume_sign
OSW chir_01   CA     N      C      CB    both
OSW chir_02   CG     CD2    CD1    CB    both
OSW chir_03   S      O1     CE2    CD1   both
#
loop_
_chem_comp_plane_atom.comp_id
_chem_comp_plane_atom.plane_id
_chem_comp_plane_atom.atom_id
_chem_comp_plane_atom.dist_esd
OSW plan-1     CA 0.020
```

OSW plan-1 C 0.020
OSW plan-1 O 0.020
OSW plan-2 CG 0.020
OSW plan-2 CD2 0.020
OSW plan-2 CE2 0.020
OSW plan-2 CE3 0.020
OSW plan-2 CZ2 0.020
OSW plan-2 CZ3 0.020
OSW plan-2 CH2 0.020
OSW plan-2 S 0.020

Supplementary table 4. Investigated potential heme-mediated autooxidation products in KatG S-Trp105

Met Tyr S-Trp	no crosslink
Met Tyr (O-Trp-S)	no crosslink, C-monooxygenation
Met Tyr O=S-Trp	no crosslink, S-monooxygenation
Met Tyr (Trp-S)O_2	S-dioxygenation
Met Tyr-(Trp-S)	partial crosslink
Met Tyr-(Trp-S=O)	partial crosslink
Met Tyr-(Trp-SO_2)	partial + dioxygenation
Met +-Tyr-(Trp-S)	full crosslink, no oxygenation
Met+-Tyr-(Trp-S)O	crosslink + S-oxygenation
Met+-Tyr-(Trp-S)O_2	crosslink + S-dioxygenation

References Cited:

1. Ndzeidze GN, Li L, Steinmetz MG. Reversible triplet excitation transfer in a trimethylene-linked thioxanthone and benzothiophene-2-carboxanilide that photochemically expels leaving group anions. *J Org Chem* **83**, 8995-9007 (2018).

2. Bisht R, Popescu MV, He Z, Ibrahim AM, Crisenza GEM, Paton RS, Procter DJ. Metal-free arylation of benzothiophenes at C4 by activation as their benzothiophene S-oxides. *Angew Chem Int Ed* **62**, e202302418 (2023).

nature portfolio

Peer Review File

Single-atom substitution redirects KatG reactivity from cofactor biogenesis to stereoselective sulfoxidation

Corresponding Author: Professor Aimin Liu

This file contains all reviewer reports in order by version, followed by all author rebuttals in order by version.

Version 0:

Reviewer comments:

Reviewer #1

(Remarks to the Author)
This paper looks at the unusual Met-Tyr-Trp cross-linked cofactor in a a catalase-peroxidase (KatG) enzyme. The paper reports the replacement of Trp105 of the M-Y-W triad with a S-Trp non-canonical amino acid. The authors demonstrate that the function of the enzyme switches from cofactor-forming to sulfoxide-forming reactivity when Trp is swapped with S-Trp. They have therefore discovered a pseudo-monooxygenase activity that is switched on in the enzyme merely by replacement of the two atoms of NH with one atom of S. The conclusions that are drawn – which are supported by mass spectrometry, cryo-EM and other spectroscopic data of very convincing quality – have profound relevance for understanding of heme protein reactivity. I am therefore very supportive of the paper, and have fairly minor comments.

- The most substantive point is the switch of reactivity that is facilitated by the Trp/S-Trp swap. There is a complete (?) switch off of the cofactor formation, and a complete (?) switch on of the monooxygenase activity. And the authors have thus confirmed that the NH group of Trp is essential for cofactor formation. And yet the title of the paper doesn't quite convey these concepts. It is not, to my reading, "catalytic switching through stereoselective sulfoxidation". It is catalytic switching TO stereoselective sulfoxidation FROM cofactor formation BY Trp swaps. I ask the authors to look at the title, and make sure that the main message isn't lost. Perhaps their phase at the end of the results "single atom substitution (at Trp105?) redirects KatG reactivity ….. from X to Y" better sums it up. But it is up to the authors to decide.

- At the end of the discussion, a mechanism is presented. All very sensible, but I did feel the paper needed a figure here so that the reader can easily compare the two reactivities that are being switched on/off. I wasn't sure that step 2 of Scheme 2 was enough as it doesn't show the proposed Compound I formation. Is it possible to draw out a simple scheme where the two reactivities are clearly shown, with the common steps (Compound I formation) shown? At the very least, formation of the sulphoxide needs to be shown in full (with the heme intermediates and some arrow pushing as well??).

- I also felt that the discussion of the Fe-O-S transition state needed a picture, perhaps as part of the figure above. With this and the other pictures above, the reader would easily be able to capture the relative reactivity of the Trp residues in the similar peroxidase and KatG enzymes.

- The authors draw out comparisons with the peroxidases in the Discussion. I agree with the authors (half way down p11) that CcP and APX do typically remain unmodified under normal turnover conditions. There is, however, evidence from a while back for radical formation on Trp 51 of CcP/mutants (JMB (2003) 328, 157; Biochemistry (2009) 48, 3593) and APX (Biochemistry (2007) 46, 2174) and covalent links, even to the heme, can be formed in some cases (e.g. Biochemistry (2007) 46, 13269). At the time this work was published, much less was known on KatG and the mass spec methods have moved on – so if the authors think this is still relevant, it would be good to know what their view is on the comparisons between KatG and these reported peroxidase reactivities.

- Formation of sulphoxides, during peroxidase-catalysed of (exogenous) sulphides, has been known for a long time. Different mechanism of course, but it might just be worth flagging some of this early work (Dunford or Paul Ortiz de Montellano may have reviewed it at some point), to make the direct comparison with substrate sulphoxidation.

- Minor issue that the last 4 lines of p3 seems to repeat themselves.

- Ditto the last 4 lines of p10 (“in the absence…..”).

- A very nice paper overall.

Reviewer #2

(Remarks to the Author)
This work shows that replacing tryptophan 105 in the enzyme KatG from E.coli by the unnatural amino acid thiotryptophan predictably leads to the loss of original catalytic function, but is surprisingly accompanied by an irreversible stereoselective autooxidation of thiotryptophan. Although this a cul-de-sac for the enzyme, the observation and characterization of the thiotryptophan sulfoxide is novel.

The multi-method experimental approach is comprehensive, the experiments are meticulously executed, and the penmanship is excellent.

Minor comments are listed below.

Page 5 line 13: "but functionally significant" - The slight change in the UV/vis spectrum does not support this conclusion about functional significance (although later data does). Rephrase.

Page 4 lines 23-26: "The magnitude and pattern..." - Again, the conclusion that reactivity is redirected is not directly supported by the activity assays - they just show reduced activity, not pointing to an "alternative reaction pathway". The next section does though. I suggest rephrasing.

Page 6 line 8: "alternative, site-specific oxidative modification" - from the HPLC and UV/vis data, it is not obvious why this would indicate an oxidative modification, rather than just the aromatic substitution. Clarify. (The following sentence is clearer in this regard).

Page 7 line 26: Unclear what "Those" refers to.

Page 7 line 29: Mtb undefined.

Page 9 line 11: Define what Rz is; this might be unfamiliar to many readers

Page 10 line 22: It is a bit of a stretch to call this autooxidation of a non-functional mutant "latent catalytic plasticity".

Page 11 line 13: 43 superscript

Reviewer #3

(Remarks to the Author)
The Authors present a study where genetic code expansion has been used to replace residue Trp105 of catalase/peroxidase KatG. This residue has previously been implicated in the formation of cross-links between methionine, tyrosine and tryptophan to form the MYW peptide that is essential for the catalase activity of KatG. The formation of cross-links is proposed to occur via a radical atom that relies on hydrogen atom transfer via the indole nitrogen of trp105. Replacing this atom with S in thiotryptophan removes the hydrogen atom that is believed to be transferred in an attempt to probe the early stages of cross-link formation. However, unexpected oxygenation of the sulfur atom occurred in the variant enzyme and the authors present structural and spectroscopic data to confirm formation of a sulfoxide on thiotrp 105 and also investigate the stereochemistry of the product and show it's formation is dependent on the presenece of haem and peroxide.

I found the paper to be well written and the evidence presented to be largely compelling and fully supportive of the conclusions drawn. The cryoEM structure clearly showed the modification of Trp105 and the spectroscopy largely supported this (see comment below).

I have a few minor comments, which are more points of curiosity rather than criticisms of the work presented.

I found the substitution of trptophan with thiotryptophan an interesting choice, clearly there is a precedent for this in the literature but I wondered if there was any specific reason why the indole ring was not replaced with a benzofuran where the N is replaced by O? This should retain the chemical characteristics of thiotryptphan (aromaticity etc) but adds a heterotaom that only differs by one proton/electron. Given the general readership of nature comms I think a comment in the introduction would be appropriate.

Also are there plans to attempt the same experiment but replacing the N with P (phosphoindole) which would replace N with

an atom of the same group but with different protonation/deprotonation behaviour?

Addition of a reaction mechanism for the proposed 2-electron oxygen atom transfer similar to the scheme S1 would be a nice addition.

In figure 3 there is no indication of the peak heights in the FTIR, could this be added? Also the blue trace (free O=S-trp) is very noisy and not very convincing. The diagnostic peak is similar size to what are presumably noise peaks.

In figure 4 the legend should state the 2.22 A resolution is density modified and the resolution of the raw amps is 2.29 A. Showing density for an unmodified trp would also be a useful for comparison to that of O=S-trp.

If these comments can be addressed I have no hesitation in recommending this manuscript for submission.

NCOMMS-26-016386 - Point-by-Point Response to the Reviewers' Comments

Reviewer #1 (Remarks to the Author):

This paper looks at the unusual Met-Tyr-Trp cross-linked cofactor in a a catalase-peroxidase (KatG) enzyme. The paper reports the replacement of Trp105 of the M-Y-W triad with a S-Trp non-canonical amino acid. The authors demonstrate that the function of the enzyme switches from cofactor-forming to sulfoxide-forming reactivity when Trp is swapped with S-Trp. They have therefore discovered a pseudo-monooxygenase activity that is switched on in the enzyme merely by replacement of the two atoms of NH with one atom of S. The conclusions that are drawn – which are supported by mass spectrometry, cryo-EM and other spectroscopic data of very convincing quality – have profound relevance for understanding of heme protein reactivity. I am therefore very supportive of the paper, and have fairly minor comments.

We thank the reviewer for the very positive comments.

- The most substantive point is the switch of reactivity that is facilitated by the Trp/S-Trp swap. There is a complete (?) switch off of the cofactor formation, and a complete (?) switch on of the monooxygenase activity. And the authors have thus confirmed that the NH group of Trp is essential for cofactor formation. And yet the title of the paper doesn't quite convey these concepts. It is not, to my reading, "catalytic switching through stereoselective sulfoxidation". It is catalytic switching TO stereoselective sulfoxidation FROM cofactor formation BY Trp swaps. I ask the authors to look at the title, and make sure that the main message isn't lost. Perhaps their phase at the end of the results "single atom substitution (at Trp105?) redirects KatG reactivity ….. from X to Y" better sums it up. But it is up to the authors to decide.

We thank the reviewer for this insightful suggestion. We agree that "redirects" more accurately captures the fundamental shift in chemical outcome. We have revised the title to: **"Single-atom substitution redirects KatG reactivity from cofactor biogenesis to stereoselective sulfoxidation."** As the reviewer noted, the switch is indeed complete; we observe no MYW cofactor formation in the as-isolated S-Trp KatG, nor during in vitro reconstitution experiments.

- At the end of the discussion, a mechanism is presented. All very sensible, but I did feel the paper needed a figure here so that the reader can easily compare the two reactivities that are being switched on/off. I wasn't sure that step 2 of Scheme 2 was enough as it doesn't show the proposed Compound I formation. Is it possible to draw out a simple scheme where the two reactivities are clearly shown, with the common steps (Compound I formation) shown? At the very least, formation of the sulphoxide needs to be shown in full (with the heme intermediates and some arrow pushing as well??).

- I also felt that the discussion of the Fe-O-S transition state needed a picture, perhaps as part of the figure above. With this and the other pictures above, the reader would easily be able to capture the relative reactivity of the Trp residues in the similar peroxidase and KatG enzymes.

We have refined **Scheme 2** to include detailed arrow pushing that explicitly illustrates the two-electron nature of the sulfoxidation pathway. In Path B, we show the concerted but asynchronous transfer where one electron from the ferryl-oxo quenches the porphyrin pi-cation radical, while the sulfur lone pair initiates an attack on the iron-bound oxygen. This provides a clear electronic rationale for why the transition state is assigned as an Fe(IV) species with a single Fe-O bond at one side and a dashed bond between the S and O. This mechanistic detail

contrasts with the one-electron radical propagation seen in the native Path A. This distinguishes the two-electron OAT in the S-Trp variant from the one-electron HAT steps in the native enzyme.

- The authors draw out comparisons with the peroxidases in the Discussion. I agree with the authors (half way down p11) that CcP and APX do typically remain unmodified under normal turnover conditions. There is, however, evidence from a while back for radical formation on Trp 51 of CcP/mutants (JMB (2003) 328, 157; Biochemistry (2009) 48, 3593) and APX (Biochemistry (2007) 46, 2174) and covalent links, even to the heme, can be formed in some cases (e.g. Biochemistry (2007) 46, 13269). At the time this work was published, much less was known on KatG and the mass spec methods have moved on – so if the authors think this is still relevant, it would be good to know what their view is on the comparisons between KatG and these reported peroxidase reactivities.

We appreciate the reviewer pointing out these critical precedents. The radical formation on Trp51 in CcP and the covalent heme-links in APX mutants demonstrate the high reactivity of these distal tryptophans when the protein scaffold is perturbed. These cases underscore the unique "evolutionary choice" of KatG to use this reactivity for beneficial cofactor biogenesis rather than deleterious off-pathway modifications. We have added a discussion of these precedents to the manuscript, noting that while one-electron chemistry is seen in CcP/APX mutants, the redirection to a two-electron oxygenation in our KatG S-Trp variant represents a distinct catalytic "switch" revealed by single-atom precision. Additionally, we have compared a recent report of human indoleamine 2,3-dioxygenase (IDO), which can take free S-Trp as an alternate substrate and inserts one oxygen into its carbon but not sulfur. We added a discussion (the second last paragraph of the Discussion section) and cited these references on page 12.

- Formation of sulphoxides, during peroxidase-catalysed of (exogenous) sulphides, has been known for a long time. Different mechanism of course, but it might just be worth flagging some of this early work (Dunford or Paul Ortiz de Montellano may have reviewed it at some point), to make the direct comparison with substrate sulphoxidation.

We have included citations to the seminal work by Dunford and Ortiz de Montellano regarding peroxidase-catalyzed sulfoxidation of exogenous sulfides. We note that while substrate sulfoxidation is a known peroxidase capability, our work demonstrates the first instance of an endogenous residue being co-opted for this chemistry via genetic code expansion, transforming the enzyme's internal life cycle.

- Minor issue that the last 4 lines of p3 seems to repeat themselves.

- Ditto the last 4 lines of p10 (“in the absence…..”).

- A very nice paper overall.

We have corrected the repetitive text on pages 3 and 10. We thank the reviewer for their careful proofreading.

Reviewer #2 (Remarks to the Author):

This work shows that replacing tryptophan 105 in the enzyme KatG from E.coli by the unnatural amino acid thiotryptophan predictably leads to the loss of original catalytic function, but is surprisingly accompanied by an irreversible stereoselective autooxidation of thiotryptophan.

Although this a cul-de-sac for the enzyme, the observation and characterization of the thiotryptophan sulfoxide is novel.

The multi-method experimental approach is comprehensive, the experiments are meticulously executed, and the penmanship is excellent.

We appreciate the above positive and encouraging summary.

Minor comments are listed below.

Page 5 line 13: "but functionally significant" - The slight change in the UV/vis spectrum does not support this conclusion about functional significance (although later data does). Rephrase.

We agree that UV-vis data alone do not establish functional significance. We have rephrased this to: "...induces subtle but detectable perturbations of the heme electronic environment (where the substituted word is underlined to replace "functionally significant" in the original text).

Page 4 lines 23-26: "The magnitude and pattern..." - Again, the conclusion that reactivity is redirected is not directly supported by the activity assays - they just show reduced activity, not pointing to an "alternative reaction pathway". The next section does though. I suggest rephrasing.

We have tempered this conclusion to better reflect the logical flow of the manuscript. The text now states: "The magnitude and pattern of these changes are consistent with the effective suppression of MYW-dependent catalysis, while the specific retention of residual peroxidase activity prompted our investigation into the alternative reaction pathway characterized in the following section.

Page 6 line 8: "alternative, site-specific oxidative modification" - from the HPLC and UV/vis data, it is not obvious why this would indicate an oxidative modification, rather than just the aromatic substitution. Clarify. (The following sentence is clearer in this regard).

We agree that the term "oxidative" jumps ahead of the evidence provided by mass spectrometry. We have revised this to: "...toward an alternative, site-specific chemical modification" (where "oxidative" has been replaced).

Page 7 line 26: Unclear what "Those" refers to.

We have clarified this sentence to specify that it refers to the broader set of variants explored in literature. It now reads: "Previously reported KatG variants lacking the MYW triad exhibit ..."

Page 7 line 29: Mtb undefined.

Mtb is now defined on page 3. We appreciate catching this oversight.

Page 9 line 11: Define what Rz is; this might be unfamiliar to many readers

R_z is now defined in the revised text.

Page 10 line 22: It is a bit of a stretch to call this autooxidation of a non-functional mutant "latent catalytic plasticity".

We understand the reviewer's point that this modification represents a loss of the enzyme's primary biological function. However, the high degree of enantioselectivity observed for the sulfoxidation—driven by the specific orientation of the residue relative to the heme—suggests a sophisticated, active site-mediated transformation rather than a stochastic autooxidation. To address the reviewer's concern, we have revised "latent catalytic plasticity" to "alternative chemical capability" to more accurately describe this reprogrammed reactivity.

Page 11 line 13: 43 superscript

Response: We have reformatted the reference citation to superscript.

Reviewer #3 (Remarks to the Author):

The Authors present a study where genetic code expansion has been used to replace residue Trp105 of catalase/peroxidase KatG. This residue has previously been implicated in the formation of cross-links between methionine, tyrosine and tryptophan to form the MYW peptide that is essential for the catalase activity of KatG. The formation of cross-links is proposed to occur via a radical atom that relies on hydrogen atom transfer via the indole nitrogen of trp105. Replacing this atom with S in thiotryptophan removes the hydrogen atom that is believed to be transferred in an attempt to probe the early stages of cross-link formation. However, unexpected oxygenation of the sulfur atom occurred in the variant enzyme and the authors present structural and spectroscopic data to confirm formation of a sulfoxide on thiotrp 105 and also investigate the stereochemistry of the product and show it's formation is dependent on the presenece of haem and peroxide.

I found the paper to be well written and the evidence presented to be largely compelling and fully supportive of the conclusions drawn. The cryoEM structure clearly showed the modification of Trp105 and the spectroscopy largely supported this (see comment below).

We thank the reviewer for their positive and supportive comments. We are pleased that the reviewer found our structural and spectroscopic evidence compelling and the paper well-written.

I have a few minor comments, which are more points of curiosity rather than criticisms of the work presented.

I found the substitution of trptophan with thiotryptophan an interesting choice, clearly there is a precedent for this in the literature but I wondered if there was any specific reason why the indole ring was not replaced with a benzofuran where the N is replaced by O? This should retain the chemical characteristics of thiotryptphan (aromaticity etc) but adds a heterotaom that only differs by one proton/electron. Given the general readership of nature comms I think a comment in the introduction would be appropriate.

Also are there plans to attempt the same experiment but replacing the N with P (phosphoindole) which would replace N with an atom of the same group but with different protonation/deprotonation behaviour?

We appreciate these forward-thinking suggestions regarding the scope of genetic code expansion. We chose thiotryptophan (S-Trp) specifically because sulfur's unique redox-sensitivity enables the two-electron oxygen-atom transfer (OAT) that is central to this study—a property that the oxygen analog (benzofuran) would likely lack, Also, L-3-(3-benzofuranyl)-alanine has limited availability.

Our engineered PylRS is specific that it excludes the native Trp, indicating that it has achieved a high level of stereoelectronic complementarity for the sulfur atom. However, developing a new high-fidelity pyrrolysyl-tRNA synthetase (PylRS) for another atomic analog is a non-trivial challenge. Our current evolved PylRS/$tRNA_{CUA}$ pair exhibits exceptional orthogonality, strictly discriminating against the native indole nitrogen to achieve high stereoelectronic complementarity for the sulfur atom. As added to the text: "The PylRS active site is precisely tuned to the unique bond lengths and polarizability of its cognate ncAA (S-Trp), highlighting the single-atom precision of this approach." The significantly smaller nitrogen (approx. 71 pm) or oxygen (approx. 66 pm) analogs than S-Trp (approx. 105 pm covalent radius) likely fail to establish the requisite steric contacts and induced-fit interactions necessary for efficient aminoacetylation. At this time, no PylRS is available for incorporating O-Trp or P-Trp.

Addition of a reaction mechanism for the proposed 2-electron oxygen atom transfer similar to the scheme S1 would be a nice addition.

This is also suggested by Reviewer 1. The revised Scheme 2 has addressed this need.

In figure 3 there is no indication of the peak heights in the FTIR, could this be added? Also the blue trace (free O=S-trp) is very noisy and not very convincing. The diagnostic peak is similar size to what are presumably noise peaks.

We have updated Figure 3 to explicitly indicate that the Y-axis represents normalized absorbance. Regarding the blue trace (free O=S-Trp), it is worth mentioning that this pure amino acid sample is in a solid crystalline state, and therefore its peak intensity cannot be directly compared with that of a liquid sample (DMSO) or a lyophilized protein. While it exhibits some background features due to the high concentration required for detection in the ATR-FTIR module, the diagnostic S=O stretching vibration at 1,041 cm^{-1} is prominent and reproducible. This feature is clearly mirrored by the 1,036 cm^{-1} peak in the KatG S-Trp105 variant (red trace) and is entirely absent in the WT enzyme (black trace), providing definitive spectroscopic evidence for sulfoxide formation.

In figure 4 the legend should state the 2.22 A resolution is density modified and the resolution of the raw amps is 2.29 A. Showing density for an unmodified trp would also be a useful for comparison to that of O=S-trp.

We have updated the legend for Figure 4 to clarify the resolution. It now reads: "(A) Cryo-EM map and atomic model of tetrameric KatG S-Trp105 at 2.22 Å resolution (density modified; raw map resolution 2.29 Å)".

Following the reviewer's suggestion, we have updated the original Fig. S13 that shows O=S-Trp in all four chains with a density map that attempting to fit by a Trp compared to O=S-Trp, and moved to the main text as Figure 5 for the sake of clarity (see on the next page). We replaced Fig. S13 with a side-by-side comparison of the density for the modified O=S-Trp105 against all native tryptophan residues elsewhere in the same KatG variant structure. This clearly illustrates

the additional, asymmetric density at position 105 that characterizes the sulfoxide modification. This is a brilliant move to add such a comparison. We appreciate reviewer's suggestions.

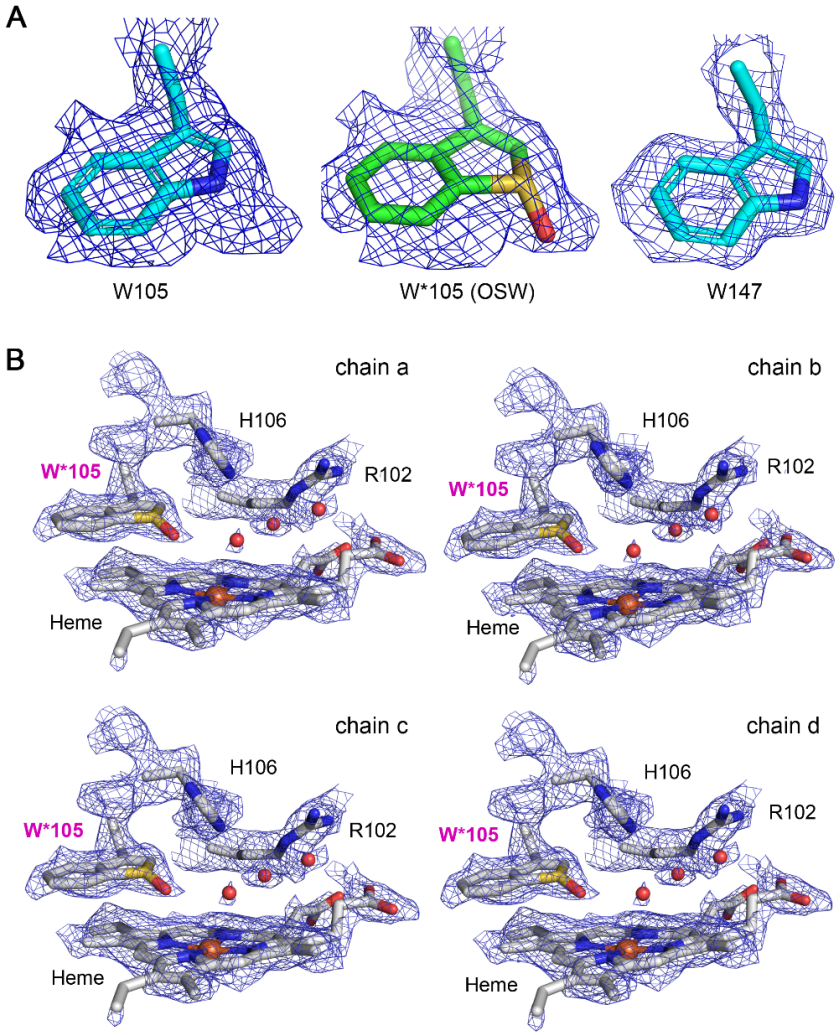

Figure 5. Stereogenic center of O=S-Trp105 in the cryo-EM structure of the engineered KatG variant. (A) Comparison of density map and model fitting on unmodified Trp, monooxygenated S-Trp (W*, molecular code in the 3D structure: OSW), and Trp147. Fig. S13 shows the comparison of O=S-Trp electron density with all other Trp residues in the same KatG structure. (B) The S-configured aromatic sulfur atom-centered configuration is uniformly observed in all four chains of the asymmetric unit. The cryo-EM density map contoured at 4.5 σ (ChimeraX).

If these comments can be addressed I have no hesitation in recommending this manuscript for submission.

Response: We appreciate your support.